NATIONAL ADVISORY COMMITTEE FOR AERONAUTICS

TECHNICAL NOTE 3711

SOME EFFECTS OF GUIDE-VANE TURNING AND STATORS ON THE ROTATING STALL CHARACTERISTICS OF A HIGH HUB-TIP RATIO SINGLE-STAGE COMPRESSOR

By Eleanor L. Costilow and Merle C. Huppert

Lewis Flight Propulsion Laboratory
Cleveland, Ohio

Washington
April 1956

NATIONAL ADVISORY COMMITTEE FOR AERONAUTICS

TECHNICAL NOTE 3711

SOME EFFECTS OF GUIDE-VANE TURNING AND STATORS ON THE ROTATING STALL CHARACTERISTICS OF A HIGH HUB-TIP RATIO SINGLE-STAGE COMPRESSOR

By Eleanor L. Costilow and Merle C. Huppert

SUMMARY

The rotating stall characteristics of several guide-vane - rotor and guide-vane - rotor - stator configurations were investigated. Guide vanes having turning angles of -22.5°, 0°, 22.5°, and 40° were used. The stage hub-tip ratio was 0.9.

Results indicate that the initial rotating stall point, number of stall zones formed, and stall propagation rate of a configuration depend not only upon blade-row inlet angle and pressure-rise characteristic, but also upon the over-all characteristics of the multiblade row unit as well. The addition of stators to a particular guide-vane - rotor configuration generally increased the flow coefficient where rotating stall was initially encountered and lowered the stall propagation rate. The number of stall zones formed in the annulus did not appear to depend upon guide-vane turning or the presence of stators.

INTRODUCTION

Several investigations of the rotating stall phenomena occurring in compressors during operation at low weight flows are reported in references 1 to 6. Rotating stall is shown to have a detrimental effect upon compressor performance since the initiation of rotating stall in the compressor is accompanied by a reduction in pressure rise. Rotating stall is also known to be a source of resonant excitation that may result in compressor blade failure such as that reported in reference 7.

This asymmetric flow problem has also been studied theoretically for a single-blade row in references 8 to 11. The rotating stall investigation of reference 6 presents in detail the rotating stall characteristics of a high hub-tip ratio rotor which approximated the stall model upon which the stall theories of references 8 to 11 were based.

This investigation is a further study of the rotating stall characteristics of multiblade-row systems obtained by the addition of a

variety of guide vanes and a set of stators to the rotor of reference 6 to make up various single-stage configurations. Thus, effects of guide vanes and stators upon the stall propagation rate, number of stall zones formed, and flow fluctuation amplitude were observed whereas other features of the rotor and test setup remained unchanged.

The rotating stall characteristics of the original stage design were also determined with an annular ring or "spoiler" inserted downstream of the stator row. The results give some indication whether the stall properties for this stage are associated with individual blade-row characteristics as well as the multiblade-row characteristics.

APPARATUS AND INSTRUMENTATION

Stage Design and Installation

Each of the following stage configurations were tested in this investigation:

Stage configuration	Guide-vane turning angle, α deg	Rotor	Stators	Annular spoiler
1	-22.5	Present	-------	-------
2	0		-------	-------
3	0		Present	-------
4	22.5		-------	-------
5	22.5		Present	-------
6	22.5		Present	Present
7	40		-------	-------
8	40		Present	-------
9	No guide vane		-------	-------

A constant hub-tip ratio of 0.9 and a casing diameter of 14 inches was maintained throughout the stage. The rotor consisted of 31 aluminum blades and the stator row, of 32 aluminum blades, both rows having NACA 65(12)-10 blower blade profiles. Thirty-eight guide vanes were used to complete the stage. The stage was originally designed for guide vanes having a turning angle of 22.5° with a symmetrical velocity diagram at the pitch radius. The vector velocity diagram for this stage configuration is given in figure 1. (All symbols used herein are given in appendix A.)

All the guide vanes with the exception of the 0° guide-vanes, which were straight vanes, were circular arc blades made from 0.06-inch sheet

steel. All blades were untwisted and untapered. For configuration 2, the 0° turning vanes had a 4-inch chord and were placed within 1/16 inch of the rotor, eliminating the usual 1/2-inch gap between guide vane and rotor rows. The straight vanes were cut back 2 inches from the leading edge for use in configuration 3. The original set of stator blades was used in all configurations that included stators.

The test setup is identical to that reported in reference 6 and is shown schematically in figure 2. Air entered through the orifice tank and a motor-driven inlet throttle into an inlet tank where screens were used to straighten the air at the compressor inlet. The air discharged into a receiver and then through an outlet throttle to the laboratory altitude exhaust system.

The annular ring or spoiler used in configuration 6 blocked approximately 50 percent of the annular area and was inserted downstream of the stage as shown in figure 3.

Flow-Fluctuation Instrumentation

A constant-temperature hot-wire anemometer system such as reported in references 12 and 13 was used to measure flow fluctuations. The wire element of the anemometer probe was made of 0.0002-inch-diameter tungsten wire mounted parallel to the probe axis and oriented in the stream so that the wire-element was not in the wake of its supports. The output signal of the anemometer was filtered electronically to exclude frequencies greater than 2000 cycles per second, which was within the flat response range of the anemometer (see ref. 13). The signal was recorded photographically from a dual-beam direct-coupled cathode-ray oscilloscope.

Hot-wire anemometer probes were installed at axial stations 2 and 4 to 8 (fig. 3). Probes were installed at several angular spacings at station 4.

Pressure-Fluctuation Instrumentation

Pressure fluctuations during stall were measured with a calibrated inductance-type pressure pickup of the kind reported in reference 14. For the purpose of the investigation, the pressure pickup was installed in the compressor casing as shown in figure 4. The pressure pickups were inserted into the compressor casing with the static tap flush with the inner surface of the compressor casing at axial stations 3 and 7 (fig. 3). Radial measurements were obtained by means of extension disks from the static tap as indicated in figure 4. The amplitude response of the pickup was flat to a frequency of 1000 cycles per second (ref. 14) and was well above the rotating stall frequencies encountered. The output of the pickup was photographically recorded from a dual-beam direct-coupled cathode-ray oscilloscope.

PROCEDURE

Steady-State Performance Characteristics

The steady-state performance of each configuration was determined in terms of static pressures. The weight flow was varied from a high value to a low flow condition by use of the outlet throttle. The static pressures were recorded photographically for several weight-flow values from a manometer board registering the static pressure from 32 static taps where four taps are located on the inner and outer casing at stations 4 to 7. When rotating stall exists in the stage, some time-average value is registered by the static taps. An absolute inlet tank pressure of 25 inches of mercury was maintained.

A preliminary investigation over a range of speeds for each configuration indicated that the stall zones propagated at a speed proportional to the rotor speed. The particular speed at which the data was taken for each configuration was selected primarily where pressure differences could be measured accurately from the manometer board. The speeds selected for each configuration are given in the following table:

Configuration	1	2	3	4	5	6	7	8	9
Corrected rotor speed, $N/\sqrt{\theta_1}$, rpm	8000	8000	8000	10,000	10,000	10,000	12,000	8000	8000

Measurement of Flow and Pressure Fluctuations

The voltage output of the hot-wire anemometer was converted to mass-flow fluctuations by the method of reference 6. The number of stall zones was found by displacing hot-wire probes around the circumference at several different angular spacings at axial station 4 and applying the analysis of reference 6. The stall frequency was determined by forming Lissajous figures on the oscilloscope with an audio-frequency oscillator. The flow fluctuations were measured at axial stations 2 and 4 to 8. The pressure fluctuations were measured at axial stations 3 and 7.

PRESENTATION OF DATA

The steady-state performance of each configuration is expressed in terms of pressure and stage inlet-flow coefficients. Presentation of the data in terms of these parameters permits quantitative comparison of the data among the configurations because the effect of differences in speed among the various configurations is essentially eliminated.

The curve showing the relation between the pressure and flow coefficient is referred to as the steady-state performance characteristic. The steady-state performance characteristic is given for the various elements of each configuration, that is, the inlet annulus, guide vane, rotor, and stator, as well as the over-all performance.

The pressure rise across the rotor is also presented in terms of cascade variables; that is, the static-pressure rise across the rotor normalized by its relative inlet dynamic head is given as a function of relative rotor inlet angle for each configuration.

The axial and radial variation in flow fluctuations due to rotating stall are given in terms of the ratio of the amplitude of the mass-flow fluctuation to the mass-flow rate indicated by the average bridge current of the hot-wire anemometer. The amplitude of the static-pressure fluctuation is given in pounds per square foot.

The stall propagation rate is presented as the ratio of absolute stall pattern rotative speed to rotor speed.

Performance and Stall Characteristics

The steady-state performance for all configurations in terms of pressure coefficient between stations 1 to 4, 4 to 5, 5 to 6, and 1 to 7 of the various stage components is presented in figure 5. The range of flow coefficient over which each stall zone pattern persisted is also indicated. A summary of the number of stall-zone patterns obtained in each configuration is given in the following table:

Configuration	1	2	3	4	5	6	7	8	9
Number of stall zones, λ	1,4	1	1	1,2	1	2,3,4	3,2,1	1,2,3	1,3,2

Rotor Pressure-Rise Coefficient

The two-dimensional pressure characteristics of the rotor (stations 5 to 6) at midspan ($r = 0.95$) in terms of cascade parameters is given in figure 6. The relative rotor-inlet angle at which rotating stall initially began is indicated in figure 6 and summarized in the following table:

Configuration	1	2	3	4	5	6	7	8	9
Initial stall angle, β, deg	56	53.5	54	78	61	74.5	81	69	52.2

Flow Fluctuations Due to Rotating Stall

The amplitude of the flow fluctuation for each configuration (no hot-wire data was taken for configuration 6) are plotted as a function of axial and radial position in figure 7. The data were not obtained to the same extent for all configurations because of hot-wire breakage. For this reason no radial survey data was obtained for configuration 7. The axial surveys were made at the mean radius ratio, r = 0.95; the radial surveys were taken at the axial station where hot-wire breakage could be kept at a minimum. This station varied from one configuration to another.

Pressure Fluctuations Due to Rotating Stall

The pressure fluctuation amplitudes measured at stations 3 and 7 for each stage configuration, are given in table I. The pressure fluctuation amplitudes were essentially constant over the radius in every case.

Stall Propagation Rates

The absolute stall propagation rates for each configuration are plotted as a function of flow coefficient in figure 8.

RESULTS AND DISCUSSION

Inasmuch as an investigation of the rotating stall characteristics of the nine configurations was the primary objective of this investigation, a discussion of the steady-state performance characteristics will be found in appendix B.

Initial Rotating Stall Point

The flow coefficients where rotating stall developed and where stall pattern changes occurred are indicated in figure 5. It is observed that rotating stall is initiated at successively lower flow coefficients as guide-vane turning is increased from -22.5° to 40°. Also the addition of stators to a particular guide-vane turning configuration caused rotating stall to occur initially at either the same flow coefficient as in the case of configurations 2 and 3 (zero guide-vane turning angle) or at a higher flow coefficient (comparing configurations 4 with 5 and 7 with 8) than without stators.

The rotor relative inlet-air angle is related to the flow coefficient and guide-vane turning by equation (B11). The inlet-air angle at

which the rotor initially developed rotating stall is indicated on figure 6. The relative inlet-air angle at initial rotating stall ranges from 52° to 81° among the various configurations. This fact indicates that the initiation of rotating stall is not uniquely determined by the inlet-air angle to the rotor as hypothesized in the theories (refs. 8 to 11). From this observation, it follows that the instigation of rotating stall likewise depends upon something in addition to stator entrance angle. Evidently, the circumstances under which rotating stall develops must be dependent upon the multiblade-row characteristics as well as individual blade-row characteristics. If the instigation of rotating stall were unaffected by system changes, then a given guide-vane - rotor combination should develop rotating stall at the same flow coefficient (or relative rotor inlet-air angle) regardless of the presence of stators, and such is not the case.

A system stability criterion similar to that found in the analysis of surge in compressors may be applicable to rotating stall, since it has been established that the initiation of rotating stall is dependent upon the multiblade-row characteristics. In surge studies (ref. 15), it has been found that the flow becomes unstable if the slope of the pressure rise against weight-flow performance characteristic becomes zero or positive. Examination of the data of figure 5 indicates that all configurations develop rotating stall when the slope of the steady-state performance characteristic from stations 1 to 7 becomes nearly zero or positive.

A further investigation of stabilizing the flow to delay the development of rotating stall was made by adding a pressure-drop element in the form of the spoiler to configuration 5 so that the slope of the pressure-coefficient curve of the combination would be negative to a lower weight flow. The results obtained with this configuration, designated configuration 6, are shown in figure 5(f). From a comparison of the results shown in figures 5(e) and 5(f), the stalled portion of the steady-state performance characteristic has been decreased approximately 50 percent as a result of the spoiler addition to the system.

At the initial stall point, configurations 1 to 4 have continuous performance characteristics. For configurations 5 to 8, a discontinuous performance characteristic curve was obtained when rotating stall first occurred in the annulus. Of the latter configurations, configurations 5, 6, and 8 have a rotor (station 5 to 6) steady-state performance curve that shows a pressure increase at the discontinuity, which is a result of a large drop in pressure at the inlet to the rotor rather than a pressure increase following the rotor. These configurations include stators and the drop in pressure across the stator element at initial stall is sufficient to produce an over-all pressure drop in the stage between stations 1 to 7. Apparently, a pressure drop across the rotor element of a stage does not necessarily occur with the development of rotating stall, but there is a net loss in pressure across the stage.

Number of Stall Zones Formed

It is not apparent from the results of this investigation upon what parameters the number of stall zones formed in the annulus depend. The results obtained do indicate that the number of stall zones does not depend upon guide-vane turning or the presence of stators.

No more than three different rotating stall patterns were found in any one configuration. The number of stall zones formed ranged from 1 to 4 among the various configurations. Configurations 2 and 3 were the only ones to have a rotating stall free region between two rotating stall regions as indicated in figures 5(b) and 5(c).

Surge

As discussed in reference 5, surge may accompany rotating stall. Such a conjunction of these two unsteady flow phenomena was observed in some configurations. An audible surge was obtained with configurations 3, 6, and 8 over a small weight-flow range as the weight flow was increased from the minimal (near zero) value. Configuration 5, the original design configuration, had a mild inaudible surge over most of the rotating stall weight-flow range regardless of throttling procedure.

Flow Fluctuations Due to Rotating Stall

It has been observed from the flow fluctuation data of figure 7 that the addition of stators to a particular guide-vane - rotor combination resulted in a general increase in flow fluctuation amplitude. The flow fluctuations also increased in amplitude as guide-vane turning is increased for all configurations with -22.5° to 22.5° guide-vane turning, and decreases in amplitude when the guide-vane turning is 40°. It is interesting to note that the original stage design, configuration 5, had the highest amplitude flow fluctuations.

The axial surveys of figure 7 show that, in general, the largest amplitude flow fluctuations $\Delta\rho V$ occurred either at station 4 or 5 in all configurations.

The flow fluctuations at station 2 are of smaller amplitude than at stations 4 or 5 because the increase in annulus area at station 2 reduces the mass-flow rate $\overline{\rho V}$ to about one-third the value of $\overline{\rho V}$ in the downstream annulus. From the radial surveys, the rotating stall patterns were found to consist in all cases of total-span stall zones which were abrupt only in some cases as seen from the steady-state performance characteristics of figure 5.

Pressure Fluctuations Due to Rotating Stall

The pressure fluctuation data taken at stations 3 and 7 are summarized in table I. A quasi-steady-state analysis identical to that given in reference 6 of the large amplitude pressure fluctuations stall patterns ($\lambda = 1$) of configurations 1, 3, 5, and 9 was made. The results indicate that instantaneous pressure coefficients between stall zones correspond approximately to the steady-state values at the same steady-state flow rate. For those stall patterns where the amplitude of the pressure fluctuations in table I were less than 60 pounds per square feet, the probable inaccuracy of the pressure fluctuation measurements makes a quasi-steady-state analysis inconclusive.

Stall Propagation Rate

All stall zones were found to rotate at a speed proportional to but less than rotor speed and in the direction of rotor rotation relative to the compressor casing. Figure 8 gives the absolute stall propagation rates as a function of flow coefficient. The speed of stall propagation apparently tends to decrease with decreasing flow coefficient and also with a decreasing number of stall zones. The latter observation supports Stenning's conclusion (ref. 11) that the relative stall propagation rate ($1 - h/N$) increases with increasing stall zone size, since the stall zone increases in size as the flow coefficient or number of stall zones is reduced. The data of figure 8 shows that the addition of stators to a particular guide-vane - rotor configuration had the general tendency to reduce the stall propagation rate from the value obtained for configurations without stators.

A comparison of the Marble and Sears theories with the rotor-alone configuration, which best fits the theoretical model, is discussed in detail in reference 6. However, Marble's equation for stall propagation for the simple cascade (ref. 10) which is equivalent to that of Sears channel theory (ref. 9) for zero phase shift between inlet angle β and discharge total-pressure fluctuation can be expressed in terms of guide-vane turning angle as follows:

$$h/N = 1 - \frac{\csc 2\beta}{\tan \beta + \tan \alpha} \qquad (1)$$

A plot of h/N as a function of β (as given by eq. (1)) for various guide-vane turnings is shown in figure 9. Figure 9 indicates that for negative guide-vane turning angle (opposite to rotor rotation) a rotating stall that propagates opposite to rotor rotation ($- h/N$) is possible. No stall zones propagating opposite to rotor rotation were detected in this investigation. For configuration 1 with -22.5° guide-vane turning

angle, the initial stall angle was 56°; according to equation (1) at this condition, the absolute stall propagation rate is zero, that is, the stall zones stand still in the annulus. For this configuration, the stall zones were found to rotate at a value of 0.41 for h/N.

The stall propagation rates for all configurations are plotted in figure 9. With the exception of configuration 9 (rotor alone), the propagation rates h/N all lie in a band between 0.2 to 0.43 regardless of guide-vane turning.

SUMMARY OF RESULTS

The rotating stall characteristics of several 0.9 hub-tip ratio blade-row configurations with guide-vane turning angles of -22.5°, 0°, 22.5°, and 40° were investigated with the following results and observations:

1. The wide range in relative inlet angle to the rotor at initial rotating stall (52° to 81°) among the configurations indicates that a blade inlet-angle condition does not uniquely determine when rotating stall begins.

2. A comparison of the rotating stall characteristics of a stage with and without an exit annular area blockage indicate that the stall characteristics are dependent upon the over-all multiblade-row system characteristics. The surge flow instability criteria is evidently applicable to the incidence of rotating stall.

3. The addition of stators to a guide-vane - rotor combination resulted in an over-all increase in flow fluctuation amplitude during rotating stall.

4. The addition of stators to a guide-vane - rotor combination had the general effect of reducing the absolute stall propagation rate.

5. The number of stall zones formed in the annulus does not appear to depend upon guide-vane turning or the presence of stators.

Lewis Flight Propulsion Laboratory
National Advisory Committee for Aeronautics
Cleveland, Ohio, February 1, 1956

APPENDIX A

SYMBOLS

$f( )$	indicates functional relation with quantity in parenthesis
f_s	frequency with which stall zone passes hot-wire anemometer or pressure gage, cps
h	absolute rotative speed of a propagating stall zone, rps
M	Mach number
N	compressor rotative speed, rps or rpm as indicated
P	total pressure, lb/sq ft
p	static pressure, lb/sq ft
q	$1/2\rho_5 W^2$, lb/sq ft
r	ratio of local radius to rotor-tip radius
U	rotor blade speed, ft/sec
V	absolute velocity, ft/sec
W	relative velocity, ft/sec
α	guide-vane turning angle measured from axial direction and positive in direction of rotor rotation, deg
β	relative rotor air-inlet angle measured from axial direction, deg
Δ	denotes finite difference of quantity following
θ	ratio of compressor-inlet temperature to NACA standard sea-level temperature of 518.688° R
λ	number of stall zones in annulus
ρ	density, slugs/cu ft
$\overline{\rho V}$	mass-flow rate indicated by average current through hot wire, lb/sec/sq ft

$\Delta\rho V/\overline{\rho V}$ amplitude of flow fluctuation divided by $\overline{\rho V}$

φ flow coefficient, V_z/U_m

ψ_{k-j} pressure coefficient, $\frac{p_j - p_k}{\frac{1}{2}\rho_4 U_m^2}$

Subscripts:

k-j axial station numbers

m mean radius (r = 0.95)

z axial

1,2, ...8 axial stations (fig. 3)

APPENDIX B

Steady-State Performance Characteristics

The performance of the inlet annulus, guide vane, rotor, and stator elements of each configuration was determined as well as the over-all configuration performance.

Inlet annulus element. - Since no work is being done on the air in the inlet section (stations 1 to 4, or station 1 to 5 for configuration 9, fig. 3), the pressure drop for this element of each configuration is related to the weight flow by Bernoulli's equation if the flow is assumed isentropic. For the inlet section, Bernoulli's equation is approximately

$$P_1 - p_4 = \frac{1}{2} \rho_4 V_{z,4}^2 \left(1 + \frac{M_4^2}{4}\right) \tag{B1}$$

or expressed in terms of pressure and stage-inlet flow coefficient equation (B1) is

$$\psi_{1-4} = - \varphi^2 \left(1 + \frac{M_4^2}{4}\right) \tag{B2}$$

The steady-state performance characteristic (ψ_{1-4} against φ) should be identical for all configurations except for the Mach number term which depends on the rotative speed of the compressor. Figure 5 shows the inlet characteristic (stations 1 to 4) to be essentially the same for all configurations to the initial stall point and is in good agreement with equation (B2). When rotating stall exists, the performance characteristic ψ_{1-4} represents some time-average value of p_4 which is different from the value obtained at the same value of φ with steady flow.

Guide-vane element. - A further drop in pressure occurs across the guide vanes as a result of the reduction in flow area due to the guide-vane turning. The performance of this element can also be derived from Bernoulli's equation, thus

$$P_1 - p_5 = \frac{1}{2} \rho_5 V_5^2 \left(1 + \frac{M_5^2}{4}\right) \tag{B3}$$

or rewriting in terms of guide-vane turning angle α equation (B3) is

$$P_1 - p_5 = \frac{1}{2} \rho_5 V_{z,5}^2 (1 + \tan^2 \alpha) \left(1 + \frac{M_5^2}{4}\right) \tag{B4}$$

In terms of pressure and stage-inlet flow coefficient the above expression becomes

$$\psi_{1-5} = - \varphi^2 \left(1 + \tan^2 \alpha\right) \left(1 + \frac{M_5^2}{4}\right) \frac{\rho_5}{\rho_4}; \quad \rho_5 \approx \rho_4 \tag{B5}$$

Since $\psi_{4-5} = \psi_{1-5} - \psi_{1-4}$, the steady-state performance using equations (B2) and (B3) is

$$\psi_{4-5} \approx - \varphi^2 \left[\left(1 + \tan^2 \alpha\right) \left(1 + \frac{M_5^2}{4}\right) - \left(1 + \frac{M_4^2}{4}\right)\right] \tag{B6}$$

which, if the Mach number terms are neglected, reduces to

$$\psi_{4-5} \approx - \varphi^2 \tan^2 \alpha \tag{B7}$$

Qualitatively, equation (B7) agrees with the trends of the steady-state performance characteristic data from station 4 to 5 as shown in figure 5. Quantitatively, however, equation (B7) is not in good agreement with the data of figure 5. This difference is attributable to growth in boundary layer and the attendant loss in total pressure so that the assumption of two-dimensional isentropic flow is no longer accurate.

Rotor element. - The pressure rise across the rotor depends upon the rotor setting angle, which was kept fixed at 28.5° for all configurations, and the rotor speed (Mach number effects). When rotor performance is expressed in terms of pressure and flow coefficient, the performance is a function of guide-vane turning. To illustrate, the cascade characteristic of the rotor may be expressed by

$$\frac{\Delta p_{5-6}}{q_{m,5}} = f(\beta) \tag{B8}$$

then

$$\Delta p_{5-6} = f(\beta) \frac{1}{2} \rho_5 W_5^2 = f(\beta) \frac{1}{2} \rho_5 \left[V_{z,5}^2 + (U_m - V_{z,5} \tan \alpha)^2\right]; \quad \rho_5 \approx \rho_4 \tag{B9}$$

or, in terms of ψ and φ, equation (B9) becomes

$$\psi_{5-6} = f(\beta) \left(\varphi_5^2 \sec^2 \alpha - 2\varphi_5 \tan \alpha + 1\right) \tag{B10}$$

The relative inlet-air angle β is related to φ_5 by the following relation:

$$\beta = \tan^{-1}\left(\frac{1}{\varphi_5} - \tan \alpha\right) \qquad (B11)$$

From equation (B10), the rotor performance characteristic depends upon guide-vane turning angle as well as flow coefficient. This dependence is shown by the characteristic from station 5 to 6 (ψ_{5-6}) of figure 5.

3933

A more direct picture of the rotor performance can be obtained from examination of the relation given by equation (B8). In terms of the cascade parameter, the rotor performance is a function only of the relative air-inlet angle and therefore should be essentially the same for all configurations except for rotor-inlet Mach number effects and experimental error. The cascade characteristic of the rotor as a function of rotor inlet-air angle is given in figure 6. As shown here, the cascade characteristic of the rotor is essentially the same to the initial stall point for all configurations with three exceptions; namely, configurations 1 to 3. In the case of configurations 2 and 3 which had the 0° guide-vane turning angle, the vanes extended downstream of the normal trailing-edge limit maintained by the other guide-vane sets and partially blocked the annulus at station 5 where the static-pressure measurements before the rotor were taken. The resultant boundary layers and area-blockage reduced the static pressure at station 5 and, consequently, resulted in an excessive pressure rise across the rotor. For configuration 1, Mach number effects are significant since the negative guide-vane turning angle increases the relative rotor Mach number significantly by adding rotation to the flow in the direction of rotor rotation.

After rotating stall develops in the annulus, the true steady-state performance characteristic is no longer determinable but some time-average value is measured instead. Configurations 4 and 7 having 22.5° and 40° guide-vane turning angles, respectively, and no stators developed rotating stall at high inlet-air angles (78° and 81°, respectively) and thus the true rotor steady-state performance characteristic is best defined by these configurations. Figures 6(d) and 6(g) show that after the cascade pressure rise coefficient reaches a maximum value of approximately 0.47 it falls off as a continuous curve when rotating stall is not present in the annulus to approximately 20 percent of the peak value at $\beta = 75^\circ$.

Stator element. - Inasmuch as the stator row was essentially the same as the rotor row, its performance would be expected to be nominally the same on the cascade performance of the rotor; however, insufficient data were taken at the stator inlet (station 6) to determine the actual cascade performance. The measured steady-state performance characteristic in terms of pressure coefficient and stage-inlet flow coefficient is, however, given in figure 5(c), (e), (f), and (g).

Over-all. - The over-all configuration performance is the sum of the performance of each element of the configuration. Thus

$$\psi_{1-7} \approx \psi_{1-4} + \psi_{4-5} + \psi_{5-6} + \psi_{6-7} \tag{B12}$$

A plot of ψ_{1-7} against φ for each configuration is given in figure 5.

REFERENCES

1. Grant, Howard P.: Hot Wire Measurements of Stall Propagation and Pulsating Flow in an Axial Flow Inducer-Centrifugal Impeller System. Pratt and Whitney Res. Rep. No. 133, June 1951.

2. Iura, T., and Rannie, W. D.: Observations of Propagating Stall in Axial-Flow Compressors. Rep. No. 4, Mech. Eng. Lab., C.I.T., Apr. 1953. (Navy Contract N6-ORI-102, Task Order 4.)

3. Emmons, H. W., Pearson, C. E., and Grant, H. P.: Compressor Surge and Stall Propagation. Trans. A.S.M.E., vol. 77, no. 4, May 1955, pp. 455-467; discussion, pp. 467-469.

4. Smith, A. G., and Fletcher, P. J.: Observations on the Surging of Various Low-Speed Fans and Compressors. Memo. No. M.219, British N.G.T.E., July 1954.

5. Huppert, Merle C., and Benser, William A.: Some Stall and Surge Phenomena in Axial-Flow Compressors. Jour. Aero. Sci., vol. 20, no. 12, Dec. 1953, pp. 835-845.

6. Costilow, Eleanor L., and Huppert, Merle C.: Rotating-Stall Characteristics of a Rotor with High Hub-Tip Radius Ratio. NACA TN 3518, 1955.

7. Trewby, G. F. A.: British Naval Gas Turbines. Trans. A.S.M.E., vol. 77, no. 4, May 1955, pp. 561-590.

8. Sears, W. R.: On Asymmetric Flow in an Axial-Flow Compressor Stage. Jour. Appl. Mech., vol. 20, no. 3, Sept. 1953, pp. 442-443.

9. Sears, W. R.: A Theory of "Rotating Stall" in Axial Flow Compressors. Graduate School Aero. Eng., Cornell Univ., Ithaca (N.Y.). (Contract AF 33 (038)-21406.)

10. Marble, Frank E.: Propagation of Stall in a Compressor Blade Row. Jour. Aero. Sci., vol. 22, no. 8, Aug. 1955, pp. 541-554.

11. Stenning, Alan H.: Stall Propagation in Cascades of Airfoils. Jour. Aero. Sci., vol. 21, no. 10, Oct. 1954, pp. 711-713.

12. Ossofsky, Eli: Constant Temperature Operation of the Hot-Wire Anemometer at High Frequency. Rev. Sci. Instr., vol. 19, no. 12, Dec. 1948, pp. 881-889.

13. Laurence, James C., and Landes, L. Gene: Auxiliary Equipment and Techniques for Adapting the Constant-Temperature Hot-Wire Anemometer to Specific Problems in Air-Flow Measurements. NACA TN 2843, 1952.

14. Patterson, John L.: A Miniature Electrical Pressure Gage Utilizing a Stretched Flat Diaphragm. NACA TN 2659, 1952.

15. Pearson, C. E.: A Study of Surge in Compressors and Jet Engines. Jour. Aero. Sci., vol. 22, no. 1, Jan. 1955, pp. 10-16.

TABLE I. - PRESSURE FLUCTUATION AMPLITUDES

Stage configuration	Number of stall zones, λ	Stall frequency, f_s, cps	Flow coefficient, φ	Pressure fluctuation amplitude, station 3, lb/sq ft	Pressure fluctuation amplitude, station 7, lb/sq ft
1	1	50	0.79	95	0
	4	232	.88	54	0
2	1	48	.52	41	23
3	1	55	.68	33	14
	1	30	.50	132	36
4	1	64	.166	37	19
	2	131	.124	48	21
	1	50	.075	60	26
5	1	36	.27	128	51
7	1	84	.13	32	25
	2	164	.11	52	32
	3	250	.07	52	36
8	2	88	.27	41	32
	1	32	.124	37	40
	3	146	.24	29	31
9	2	175	.705	21	20
	3	276	.68	28	17
	1	60	.63	172	106

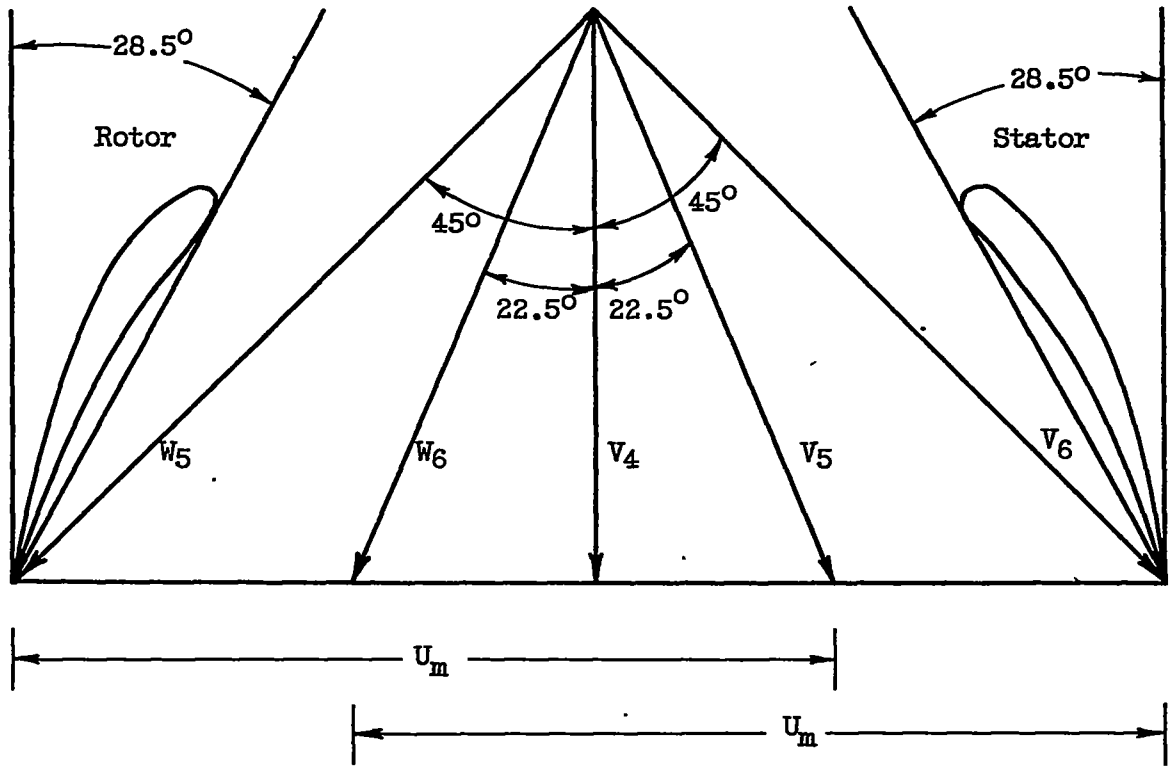

Figure 1. - Vector velocity diagram.

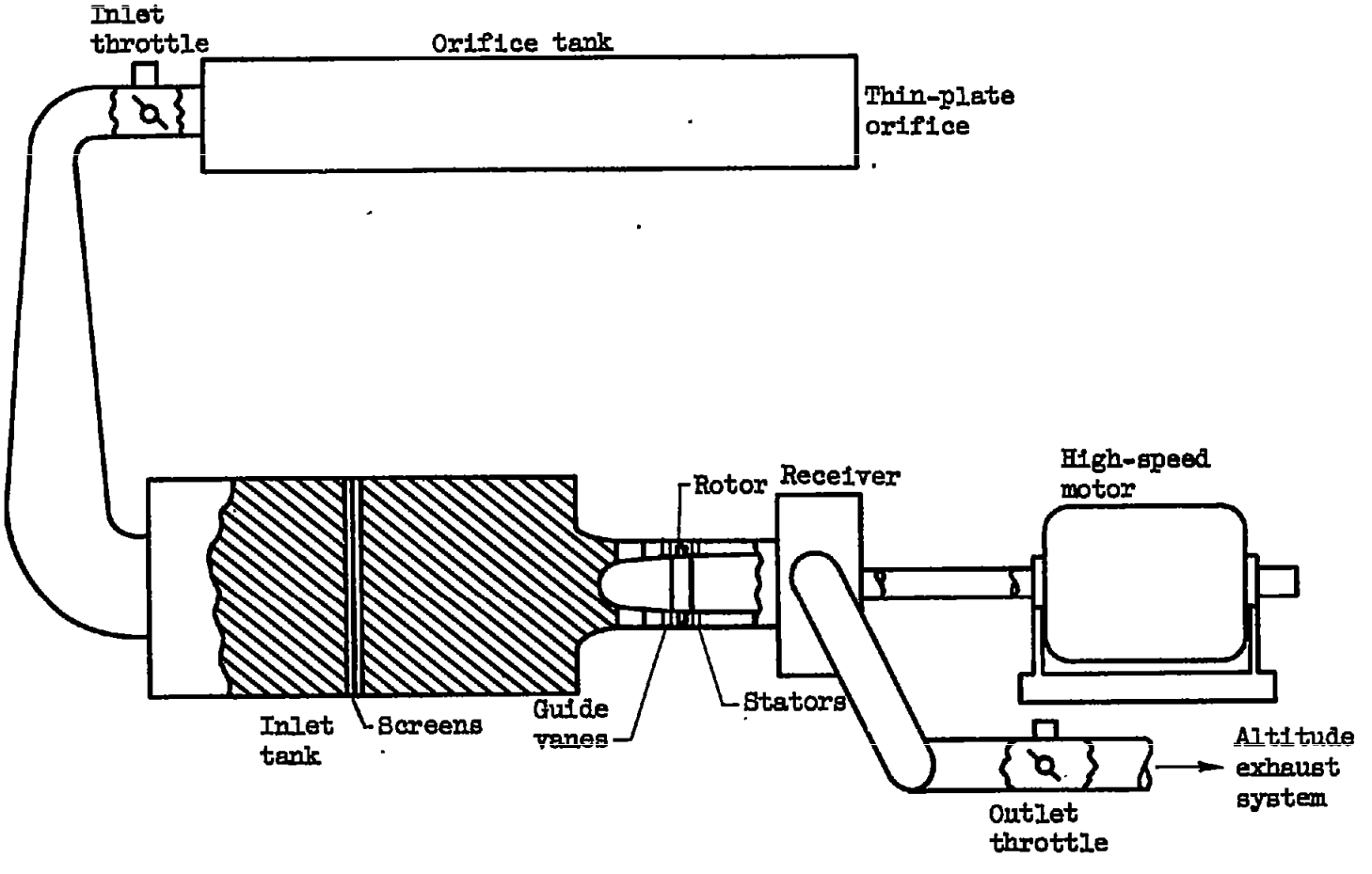

Figure 2. - Compressor installation.

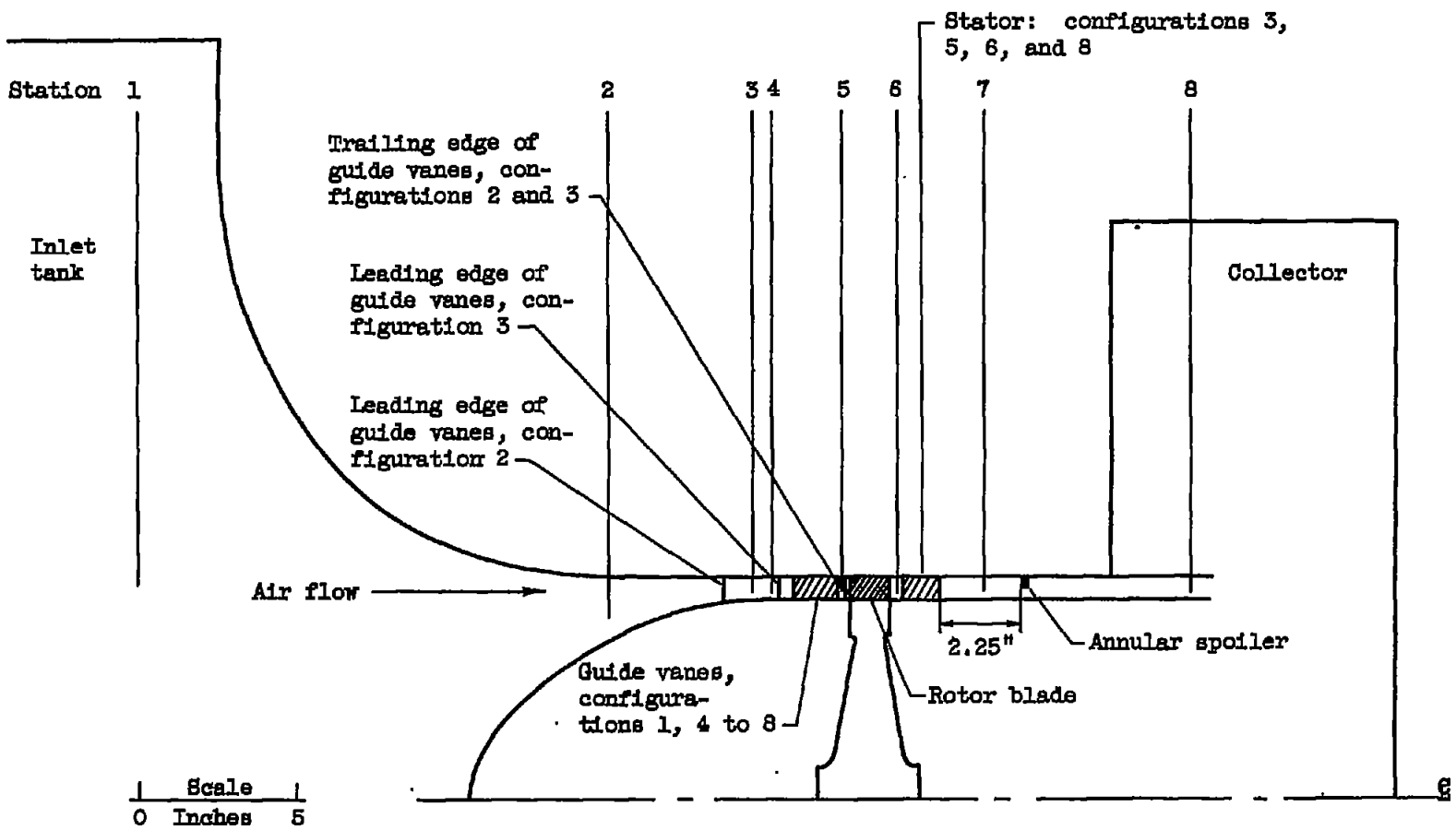

Figure 3. - Axial measuring stations and blade configurations.

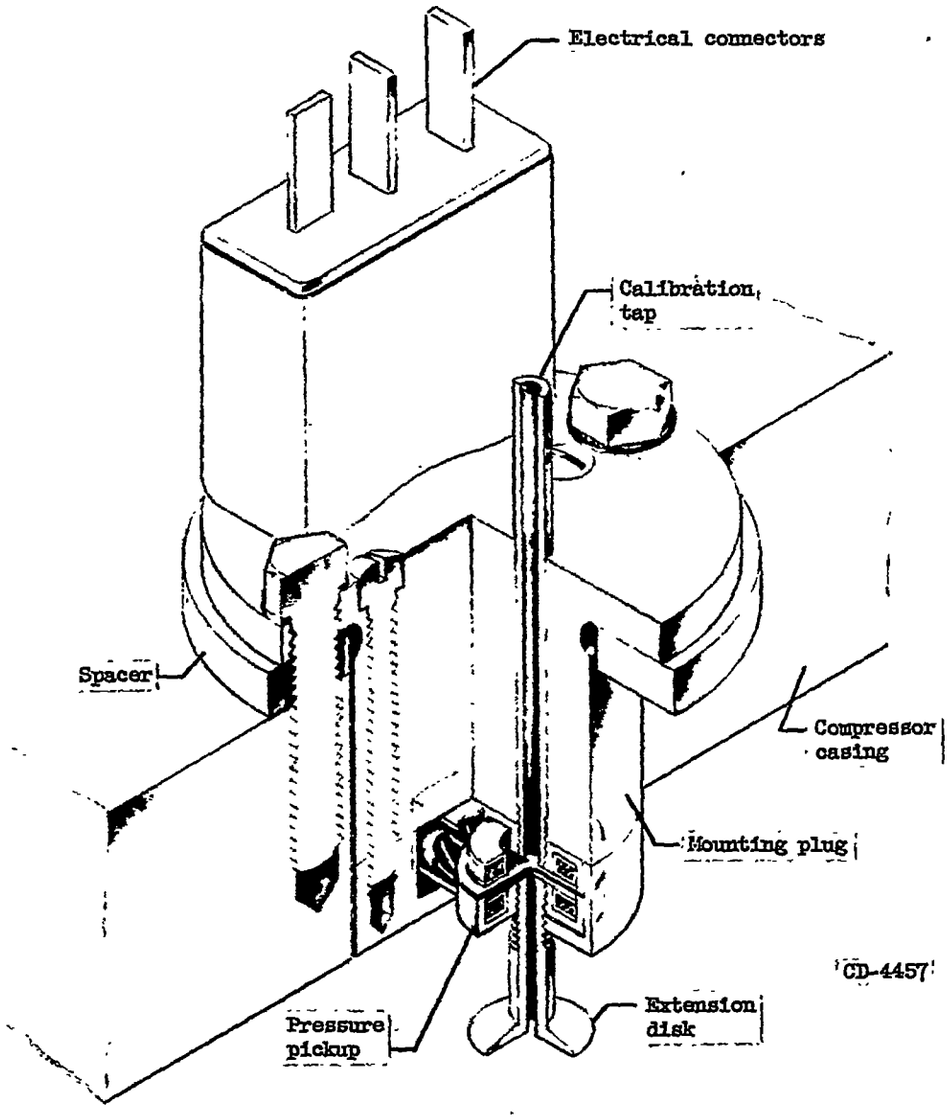

Figure 4. - Installation of pressure pickup in compressor casing.

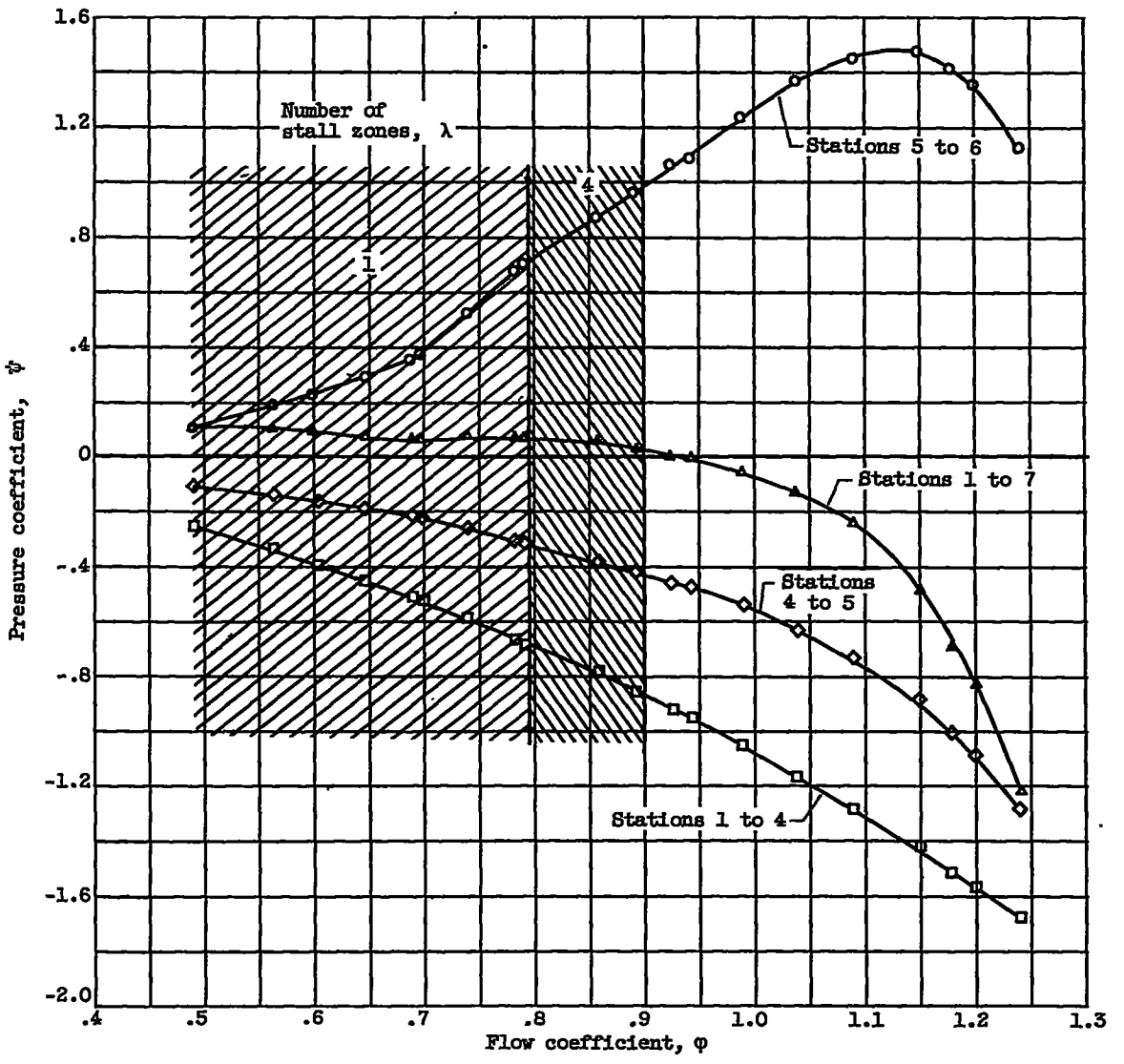

(a) Configuration 1. Guide-vane turning angle, -22.5°; no stators; corrected rotor speed, 8000 rpm.

Figure 5. - Steady-state performance and rotating stall regions.

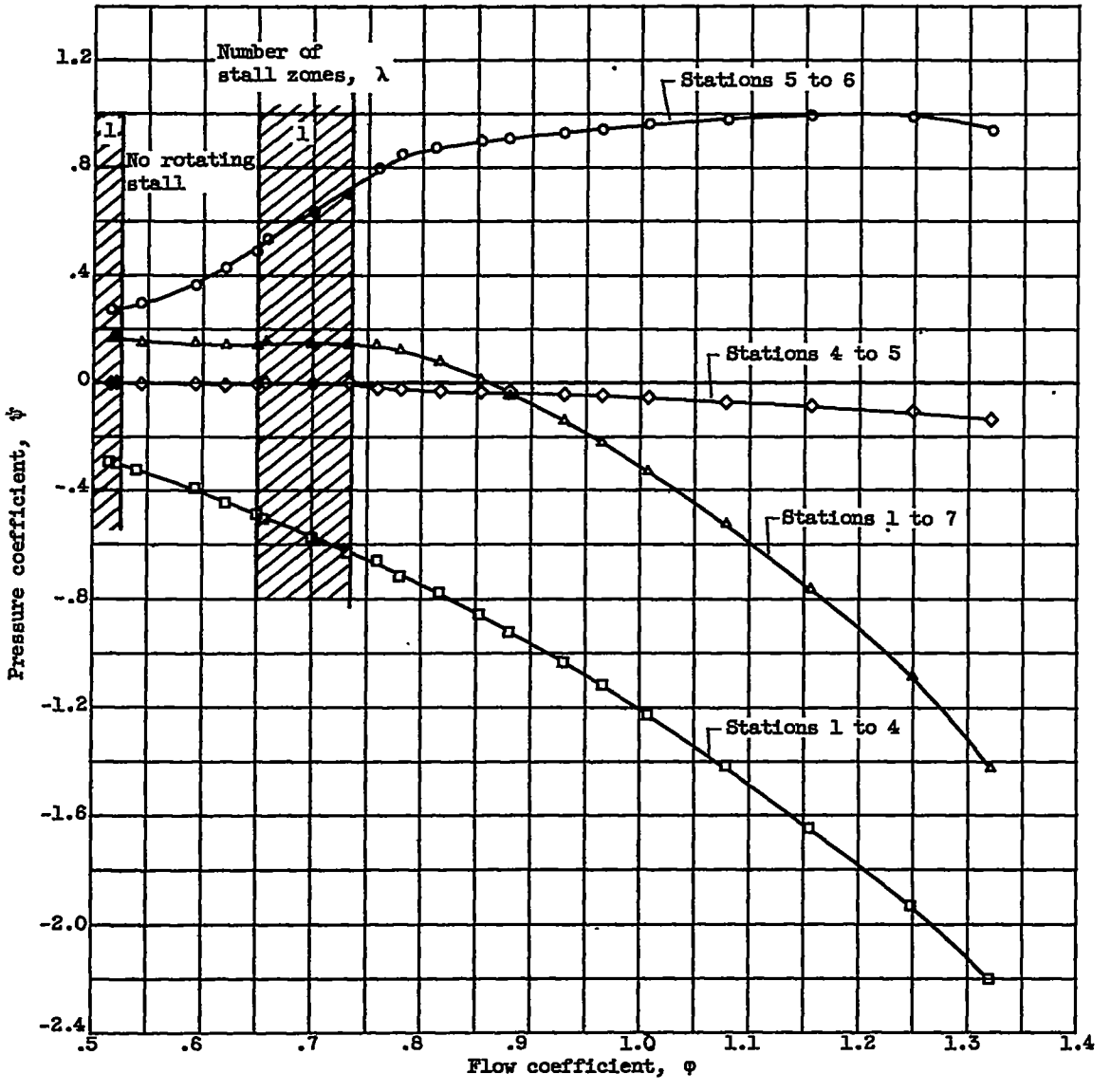

(b) Configuration 2. Guide-vane turning angle, 0°; no stators; corrected rotor speed, 8000 rpm.

Figure 5. - Continued. Steady-state performance and rotating stall regions.

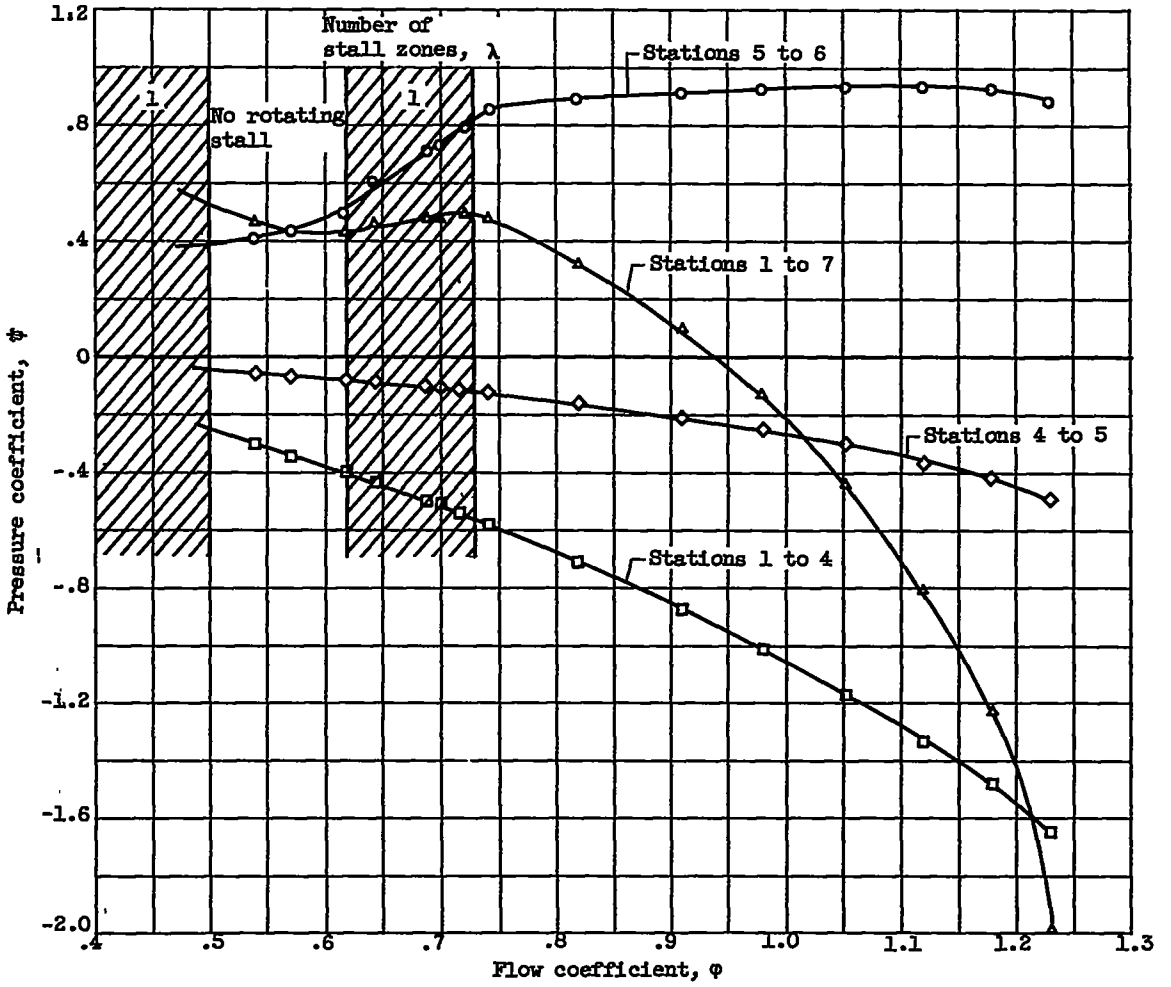

(c) Configuration 3. Guide-vane turning angle, 0°; with stators; corrected rotor speed, 8000 rpm.

Figure 5. - Continued. Steady-state performance and rotating stall regions.

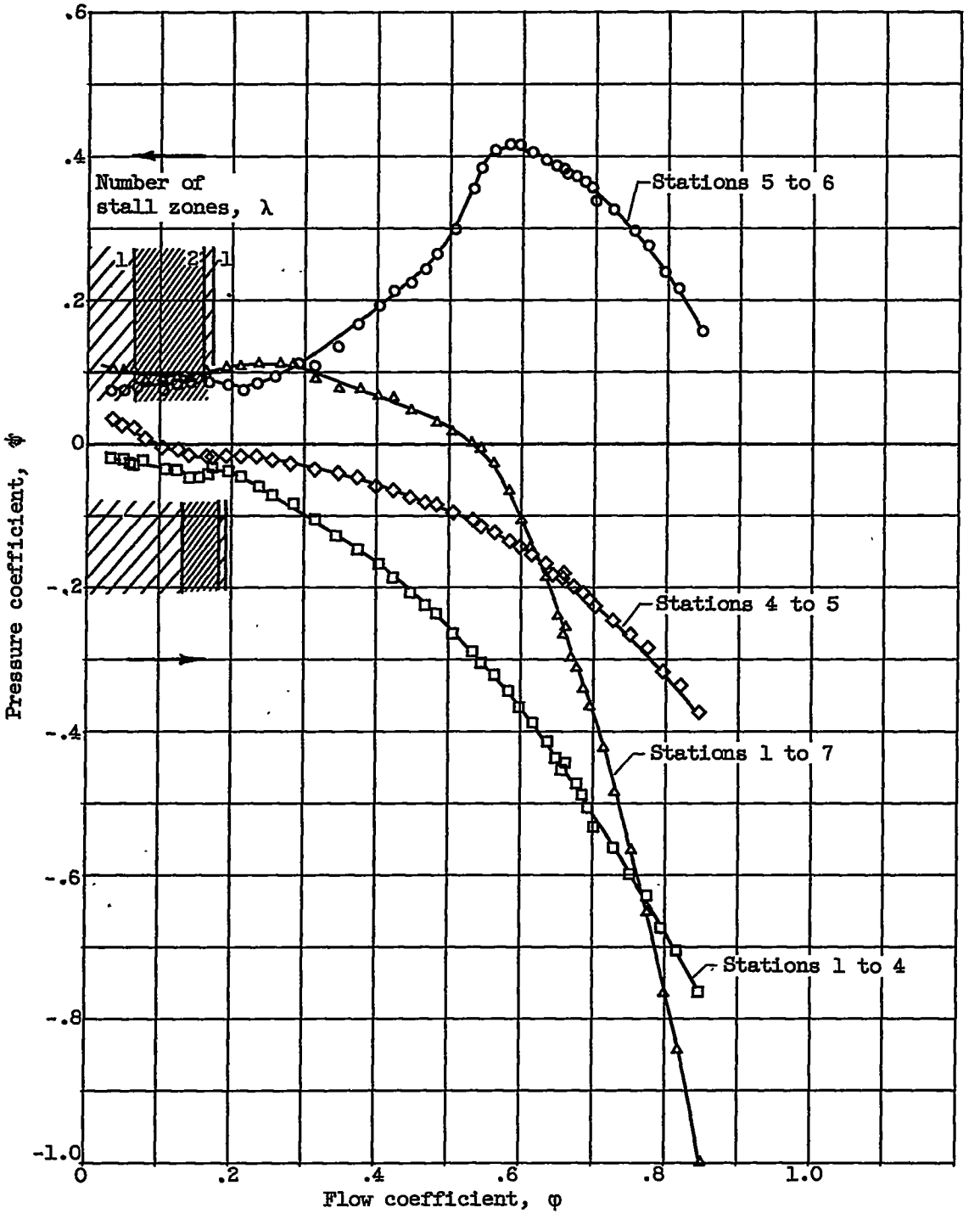

(d) Configuration 4. Guide-vane turning angle, 22.5°; no stators; corrected rotor speed, 10,000 rpm.

Figure 5. - Continued. Steady-state performance and rotative stall regions.

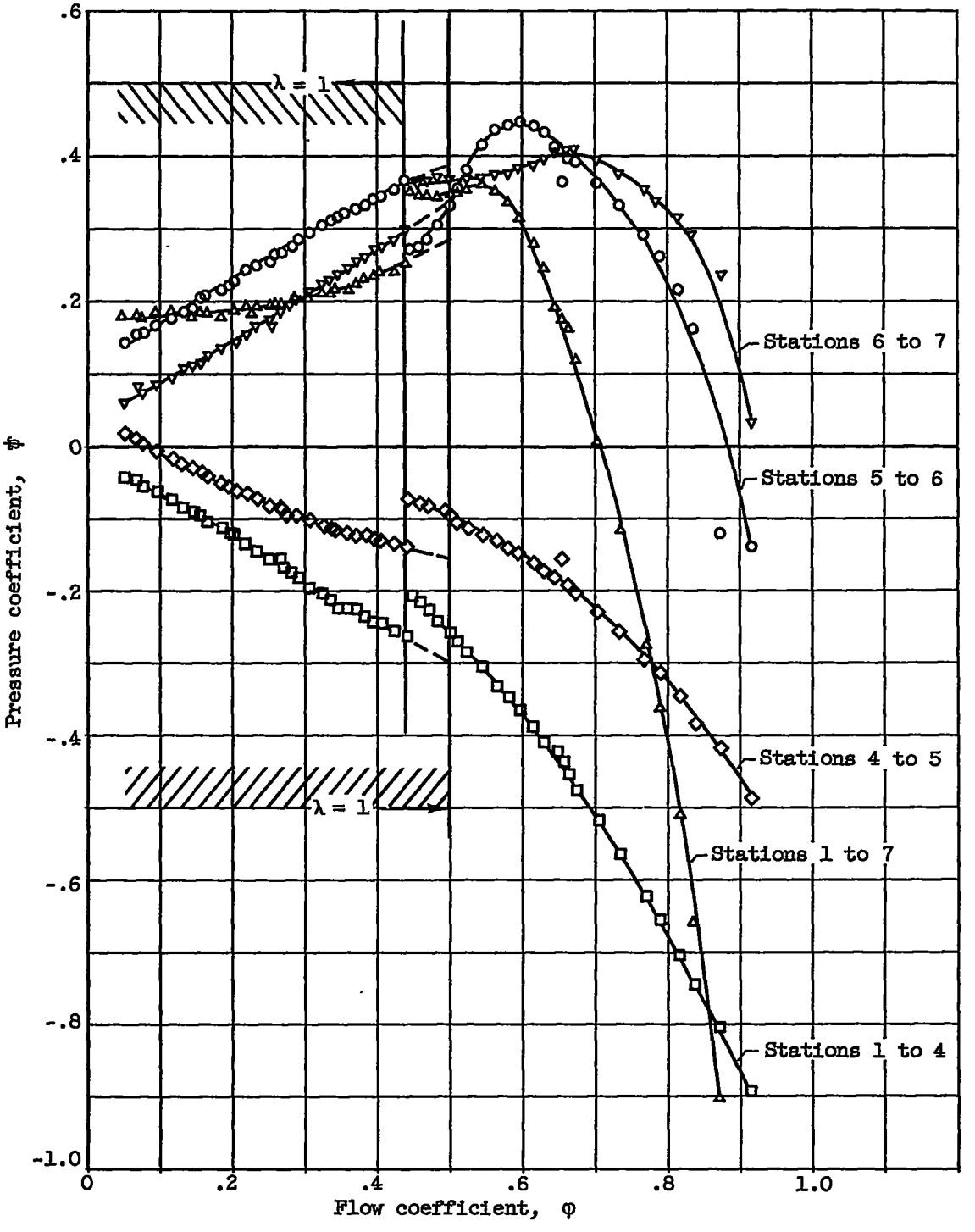

(e) Configuration 5. Guide-vane turning angle, 22.5°; stators; corrected rotor speed, 10,000 rpm.

Figure 5. - Continued. Steady-state performance and rotating stall regions.

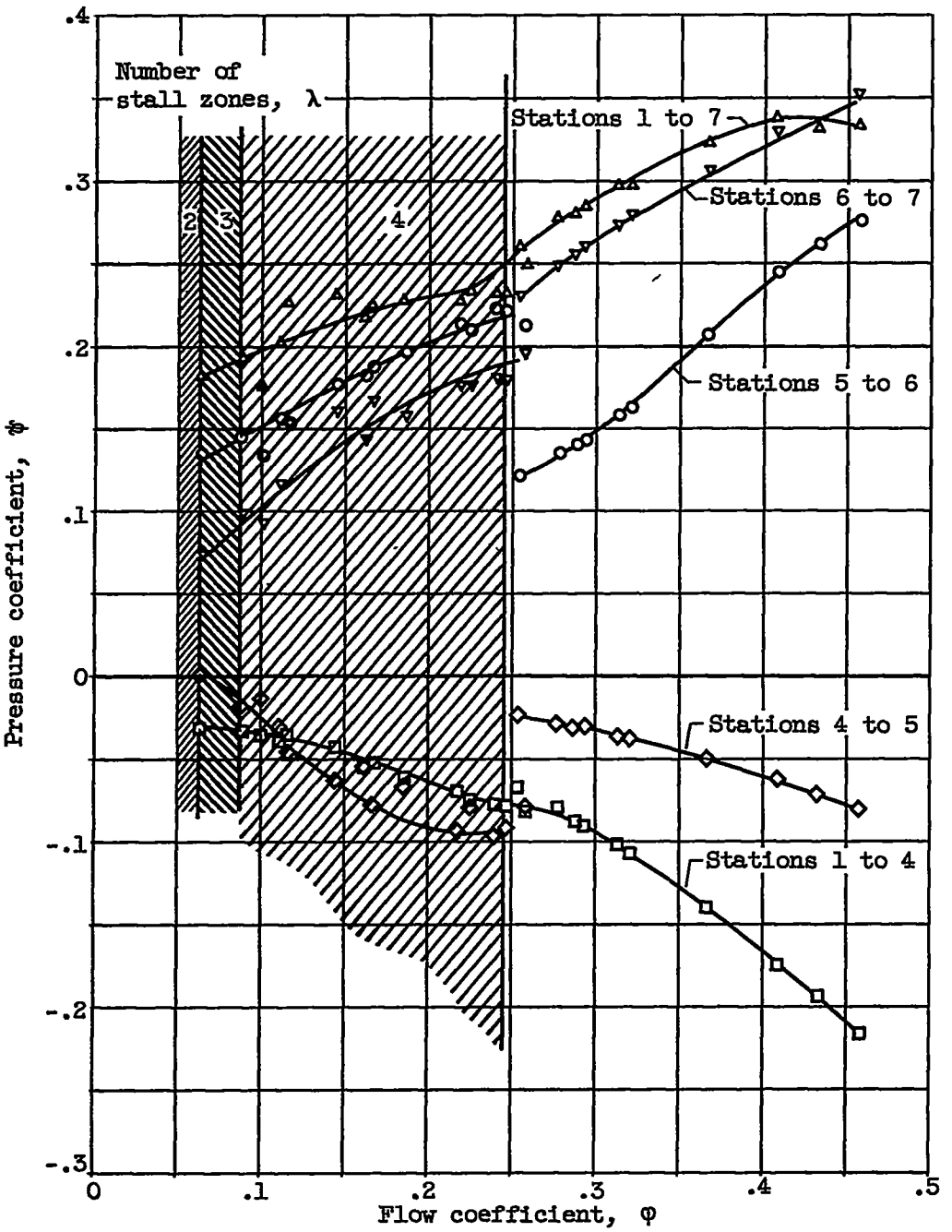

(f) Configuration 6. Guide-vane turning angle, 22.5°; stators; corrected rotor speed, 10,000 rpm.

Figure 5. - Continued. Steady-state performance and rotating stall regions.

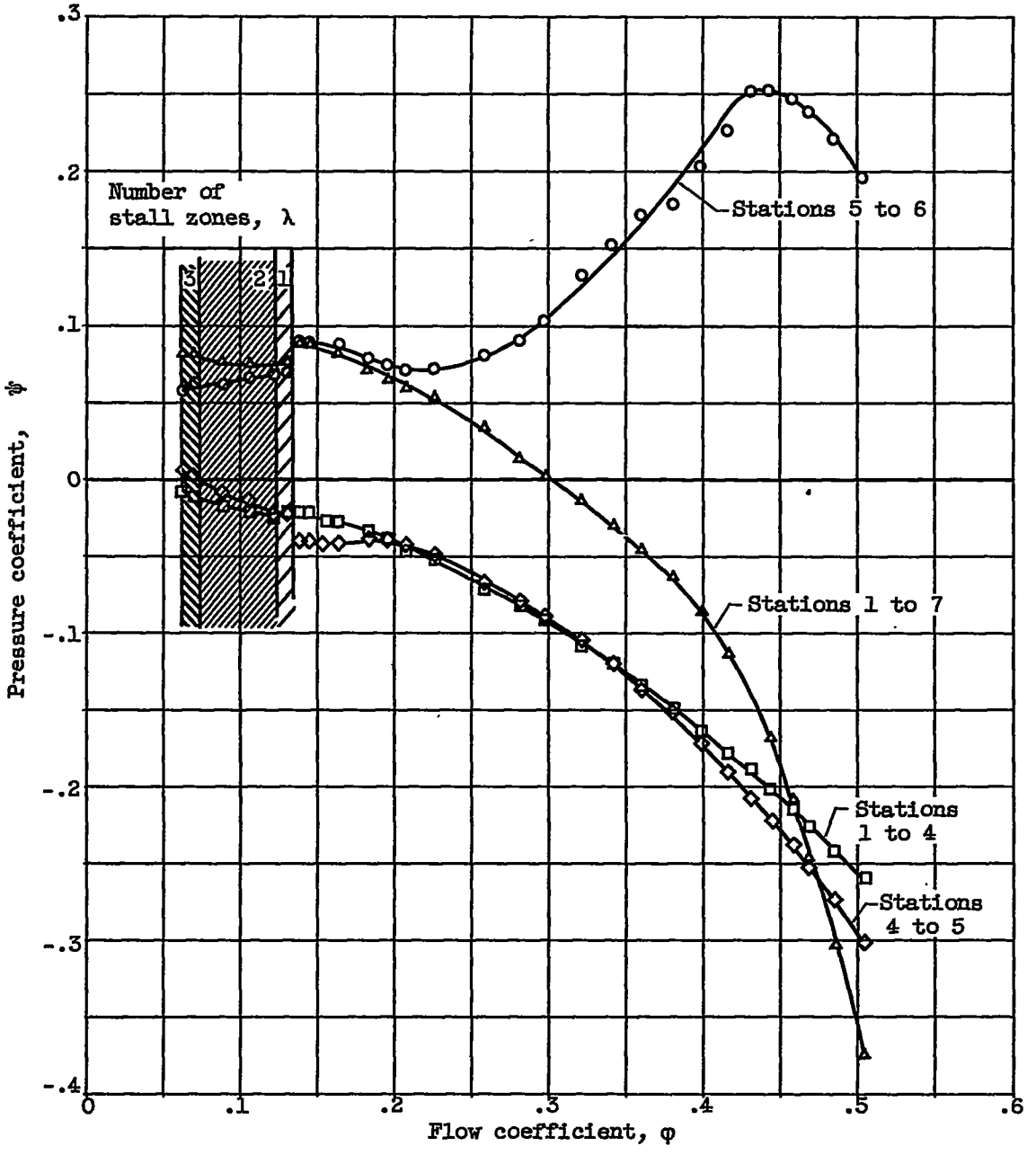

(g) Configuration 7. Guide-vane turning angle, 40°; no stators; corrected rotor speed, 12,000 rpm.

Figure 5. - Continued. Steady-state performance and rotating stall regions.

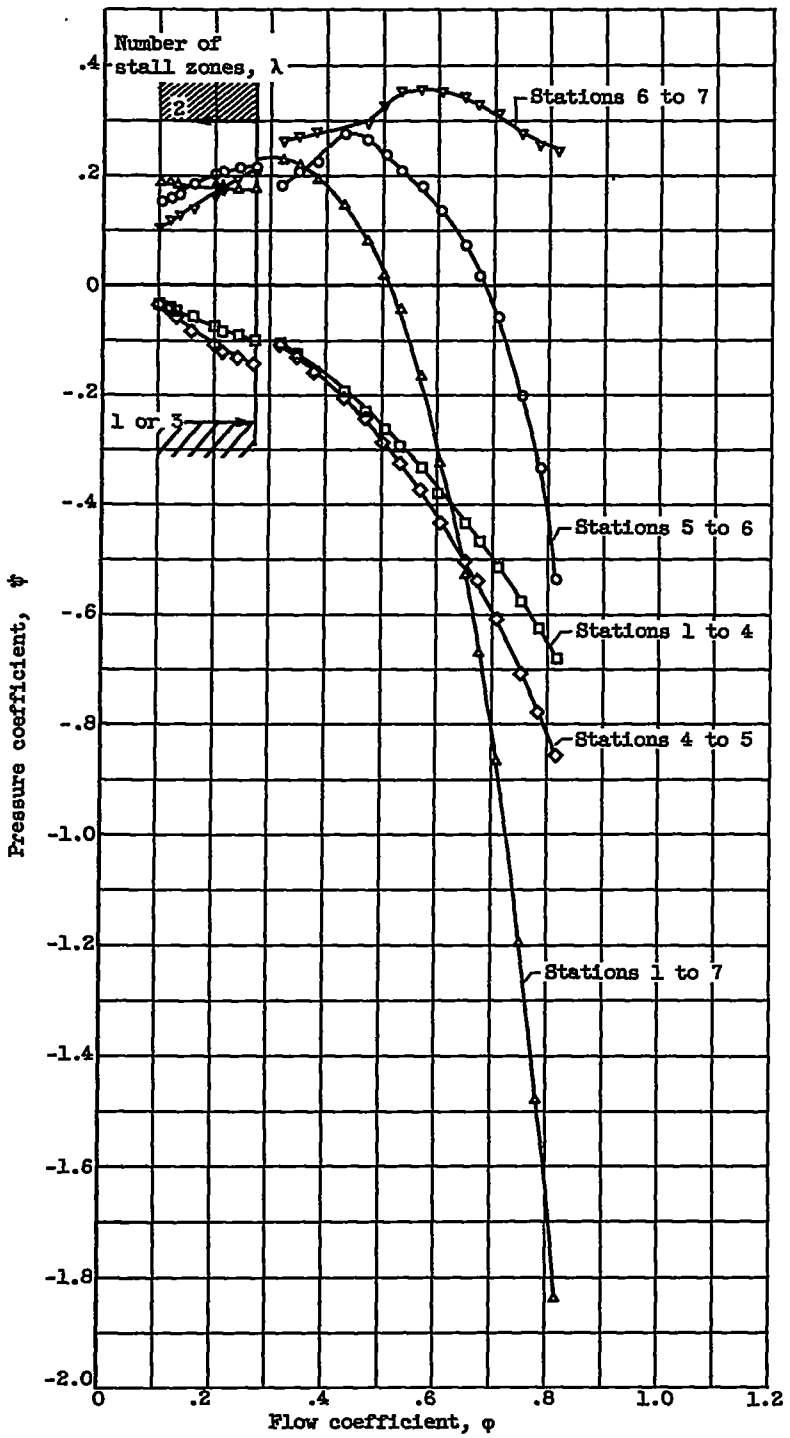

(h) Configuration 8. Guide-vane turning angle, 40°; stators; corrected rotor speed, 8000 rpm.

Figure 5. - Continued. Steady-state performance and rotating stall regions.

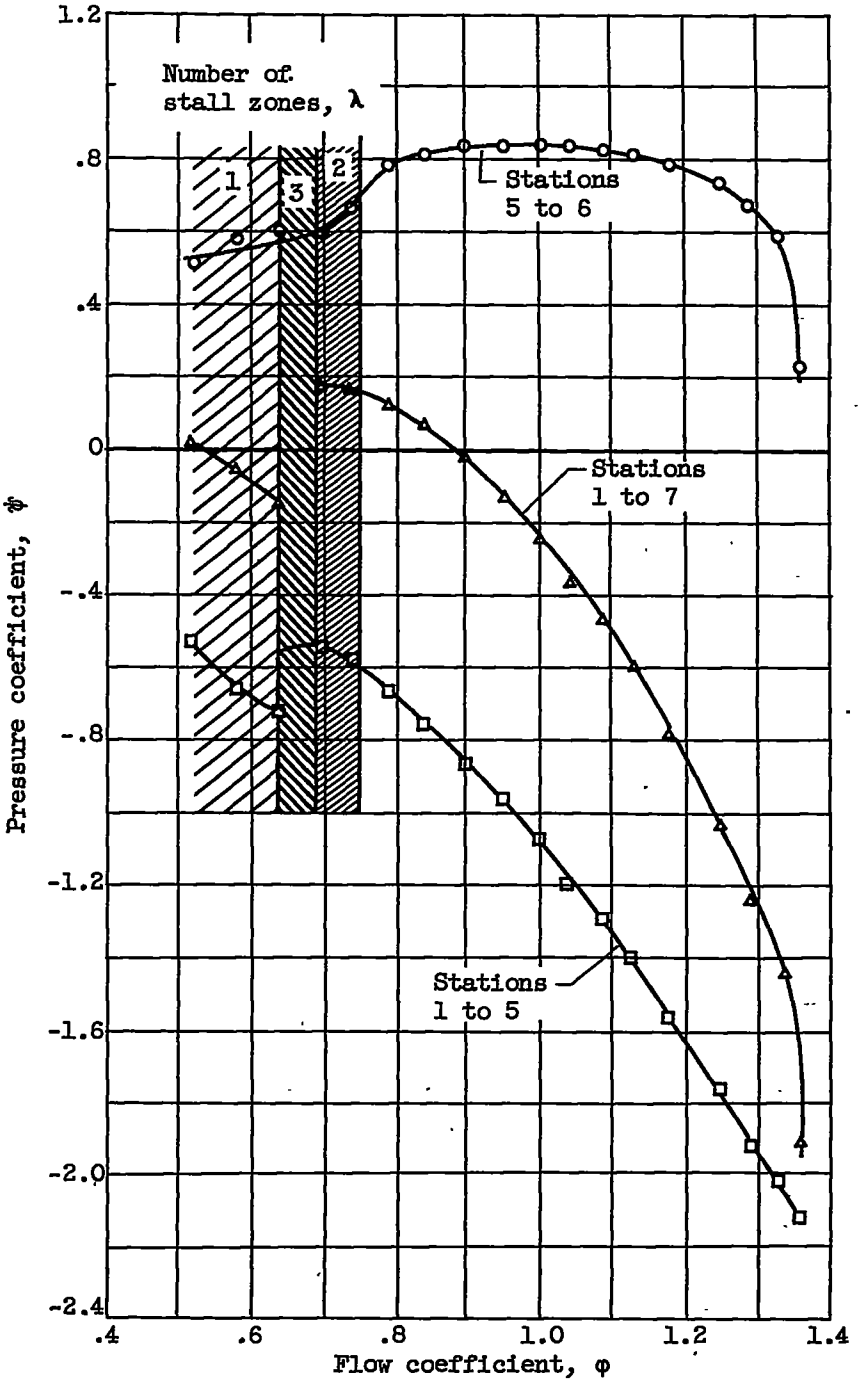

(i) Configuration 9. No guide-vane turning angle; no stators; corrected rotor speed, 8000 rpm.

Figure 5. - Concluded. Steady-state performance and rotating stall regions.

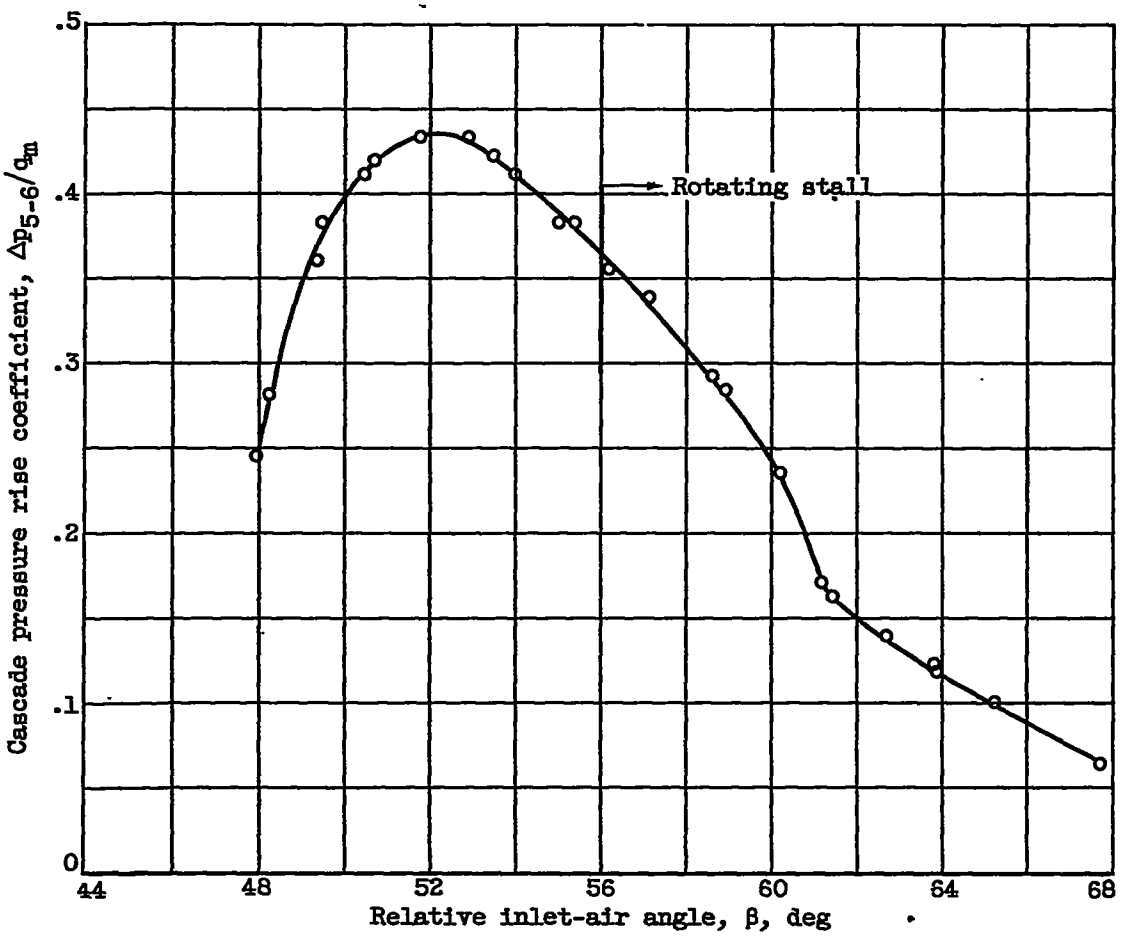

(a) Configuration 1. Guide-vane turning angle, -22.5°; no stators; corrected rotor speed, 8000 rpm.

Figure 6. - Rotor pressure-rise characteristic as function of relative inlet-air angle at mean radius ratio of 0.95.

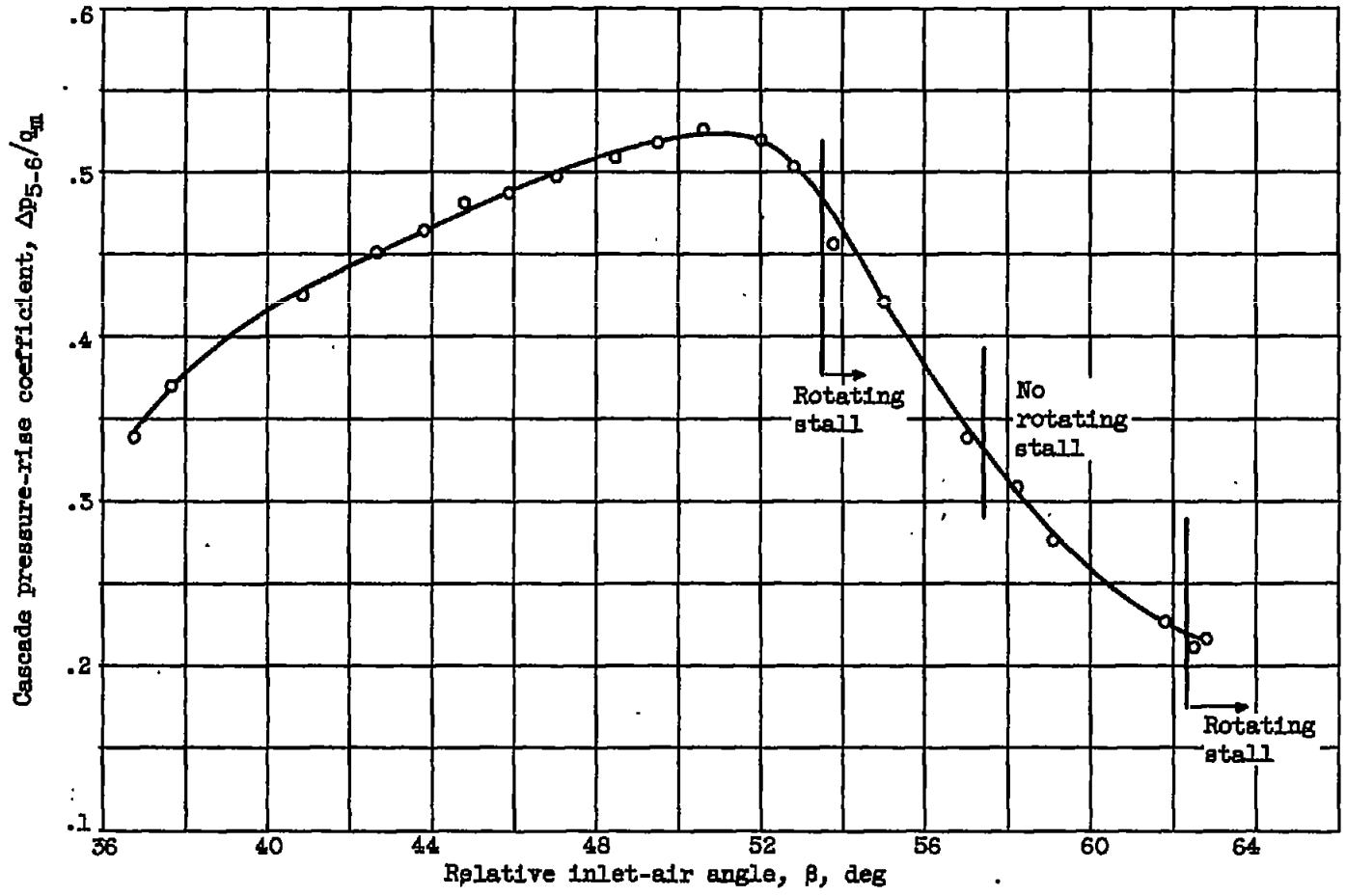

(b) Configuration 2. Guide-vane turning angle, 0°; no stators; corrected rotor speed, 8000 rpm.

Figure 6. - Continued. Rotor pressure-rise characteristic as function of relative inlet-air angle at mean radius ratio of 0.95.

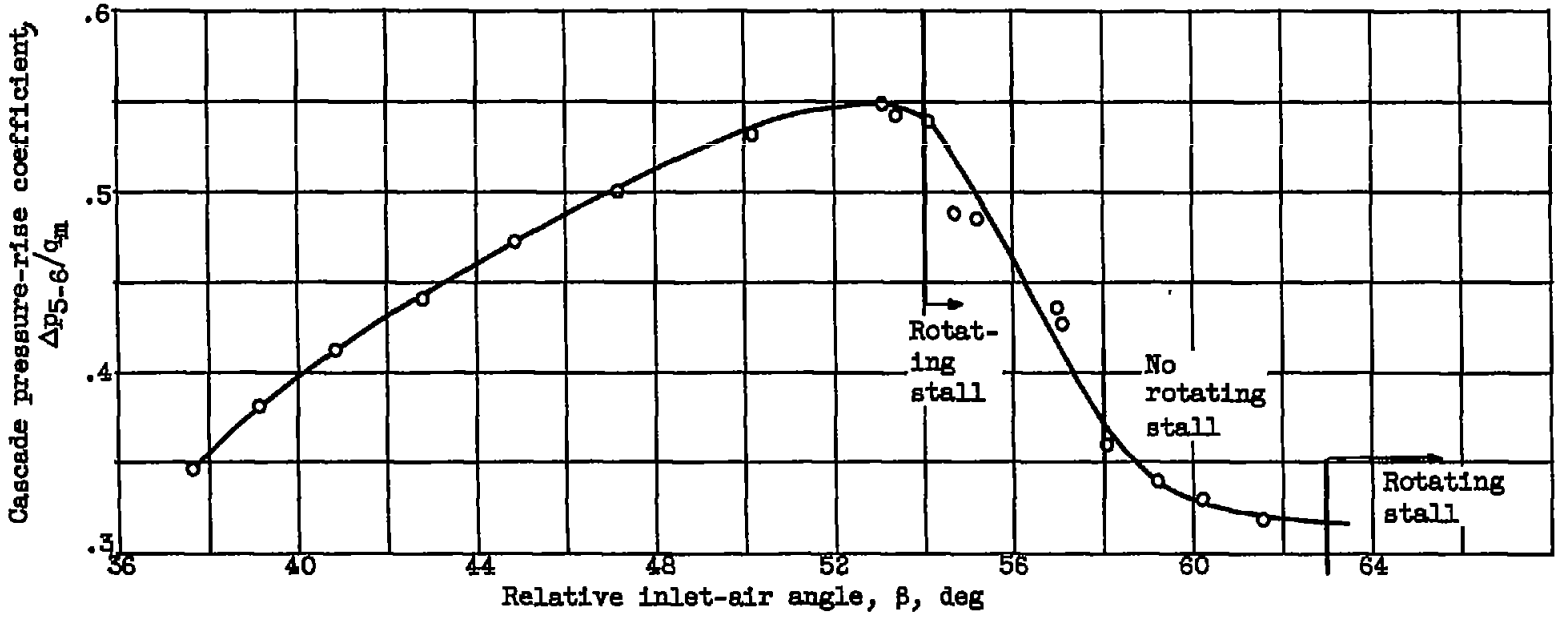

(c) Configuration 3. Guide-vane turning angle, 0°; stators, corrected rotor speed, 8000 rpm.

Figure 6. - Continued. Rotor pressure-rise characteristic as function of relative inlet-air angle at mean radius ratio of 0.95.

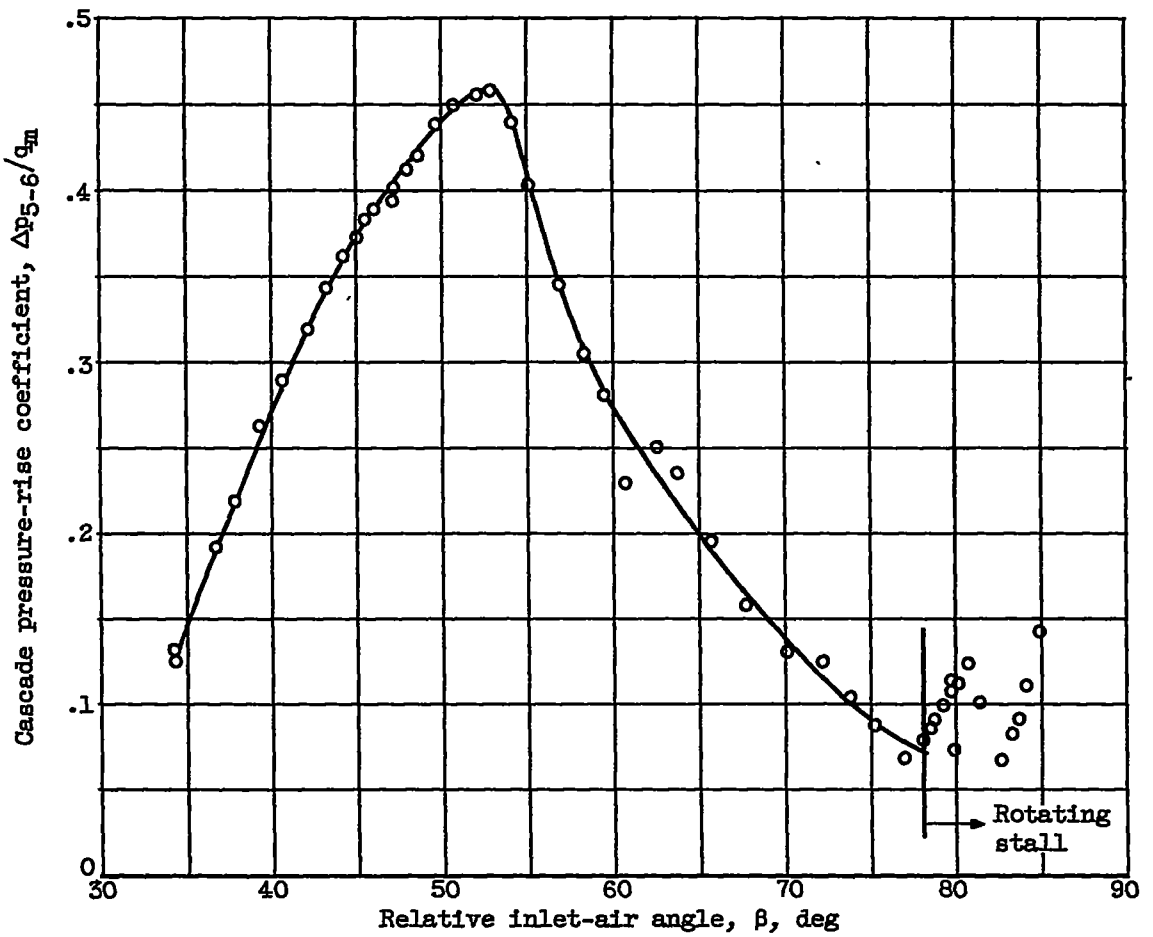

(d) Configuration 4. Guide-vane turning angle, 22.5°; no stators; corrected rotor speed, 10,000 rpm.

Figure 6. - Continued. Rotor pressure-rise characteristic as function of relative inlet-air angle at mean radius ratio of 0.95.

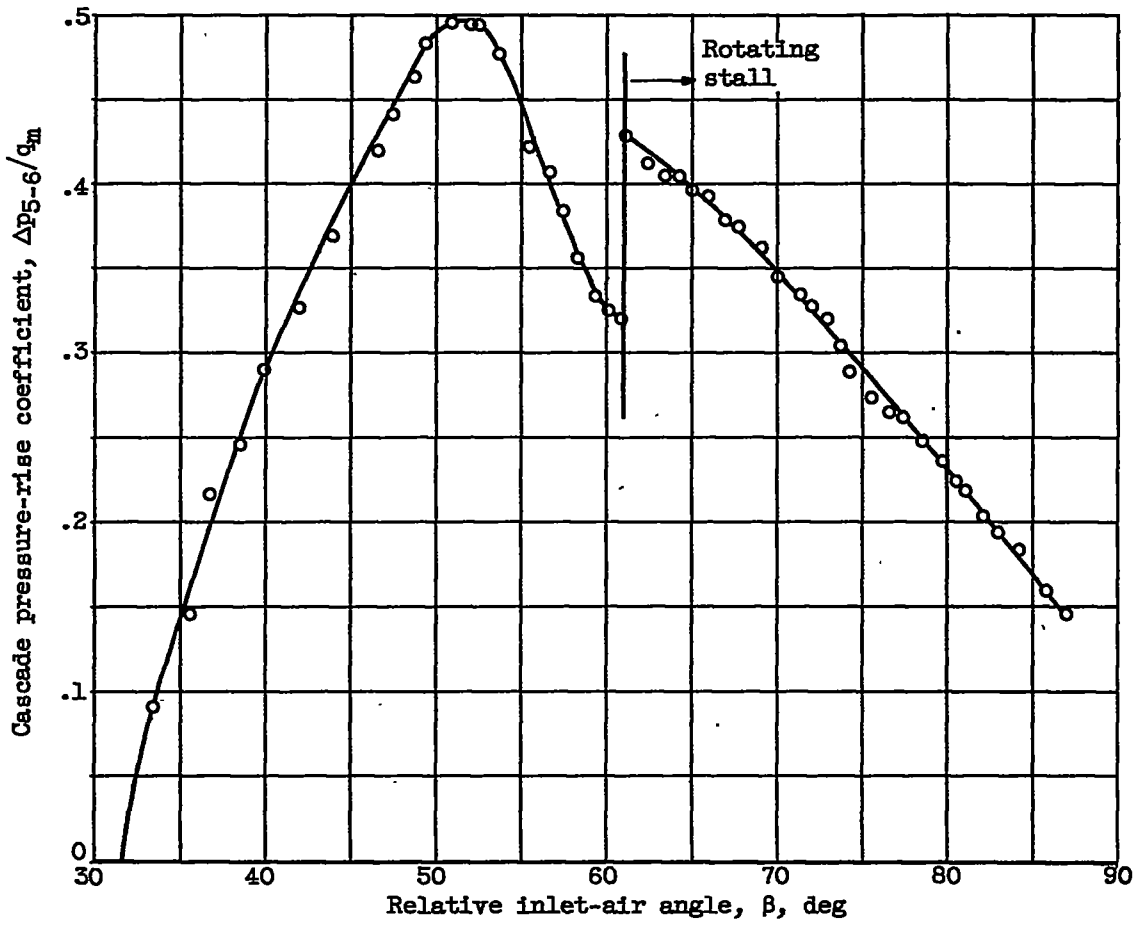

(e) Configuration 5. Guide-vane turning angle, 22.5°; stators; corrected rotor speed, 10,000 rpm.

Figure 6. - Continued. Rotor pressure-rise characteristic as function of relative inlet-air angle at mean radius ratio of 0.95.

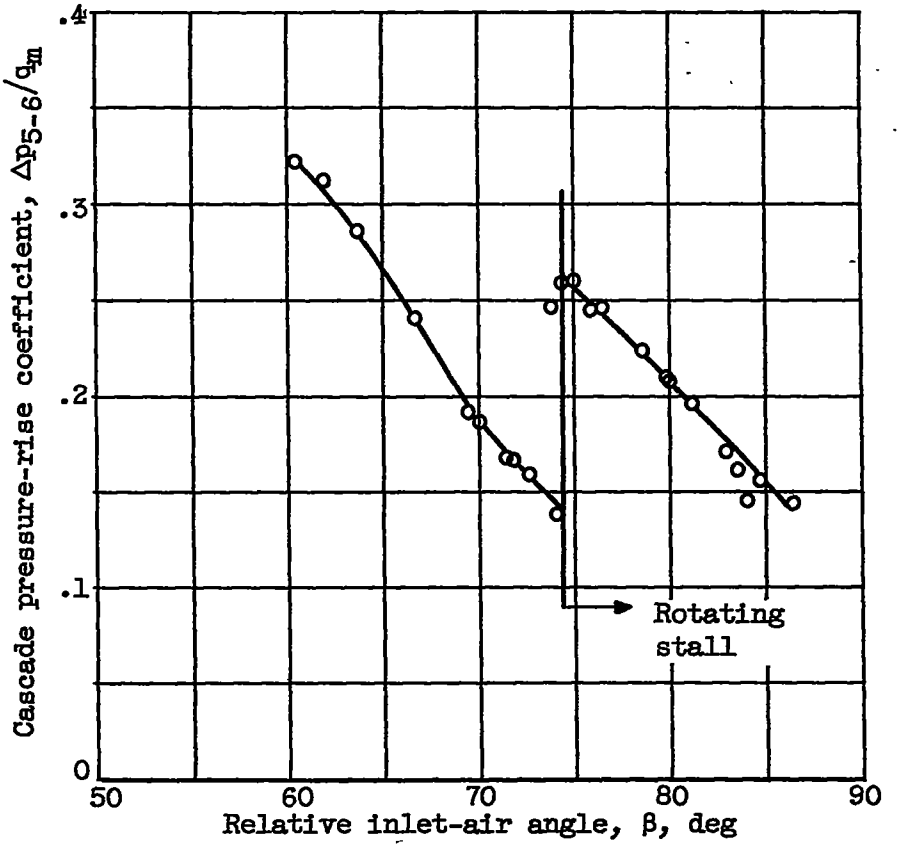

(f) Configuration 6. Guide-vane turning angle, 22.5°; stators and spoiler; corrected rotor speed, 10,000 rpm.

Figure 6. - Continued. Rotor pressure-rise characteristic as function of relative inlet-air angle at mean radius ratio of 0.95.

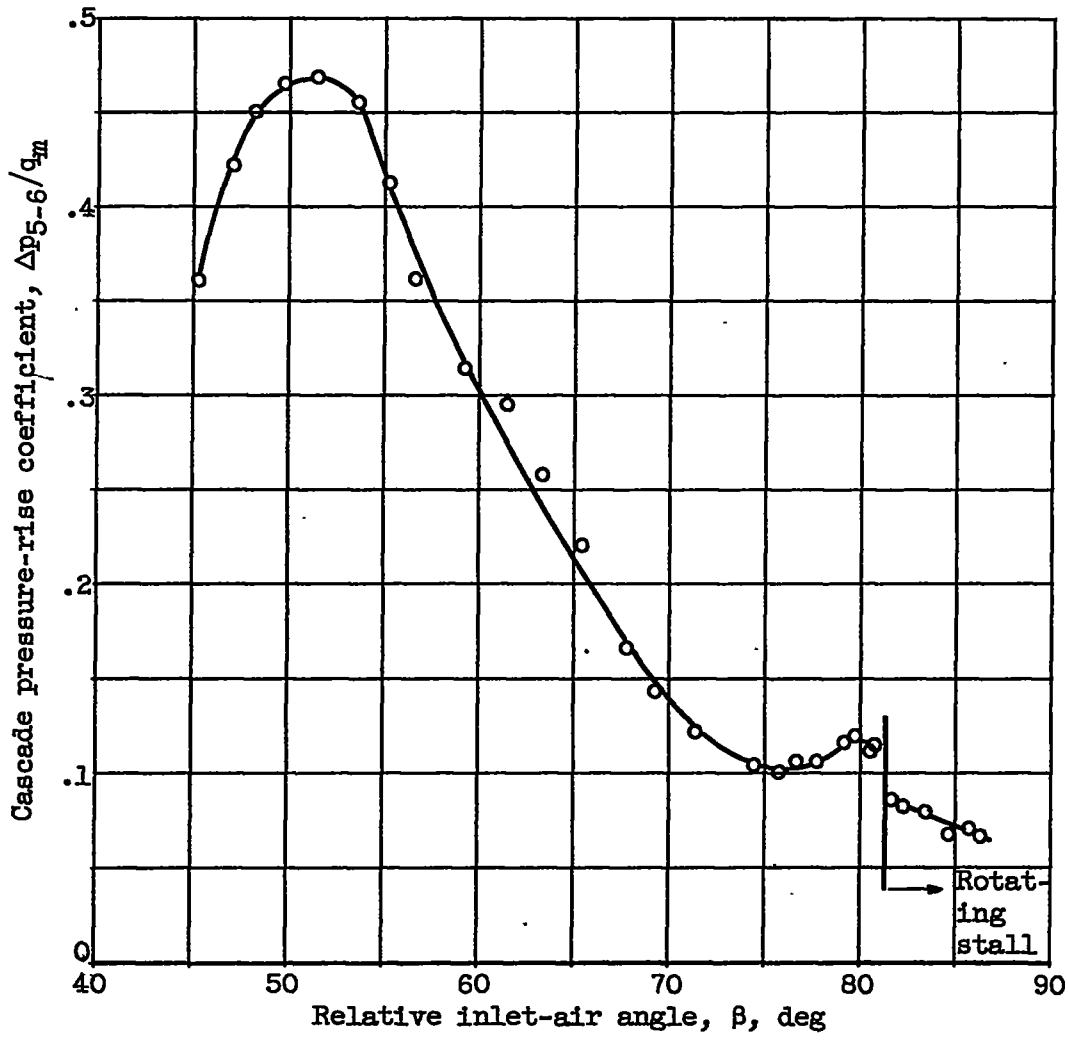

(g) Configuration 7. Guide-vane turning angle, 40°; no stators; corrected rotor speed, 12,000 rpm.

Figure 6. - Continued. Rotor pressure-rise characteristic as function of relative inlet-air angle at mean radius ratio of 0.95.

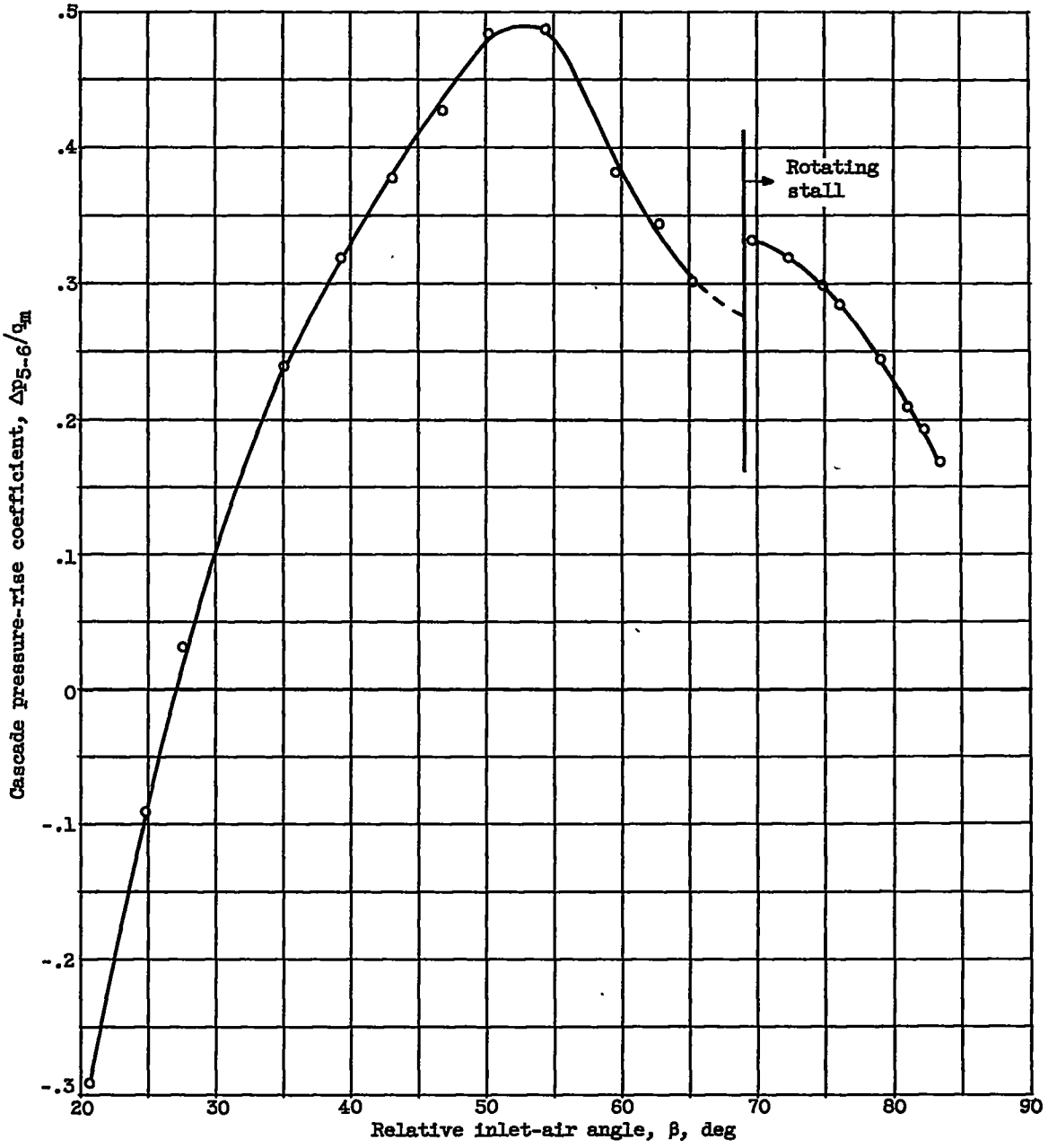

(h) Configuration 8. Guide-vane turning angle, 40°; stators; corrected rotor speed, 8000 rpm.

Figure 6. - Continued. Rotor pressure-rise characteristic as function of relative inlet-air angle at mean radius ratio of 0.95.

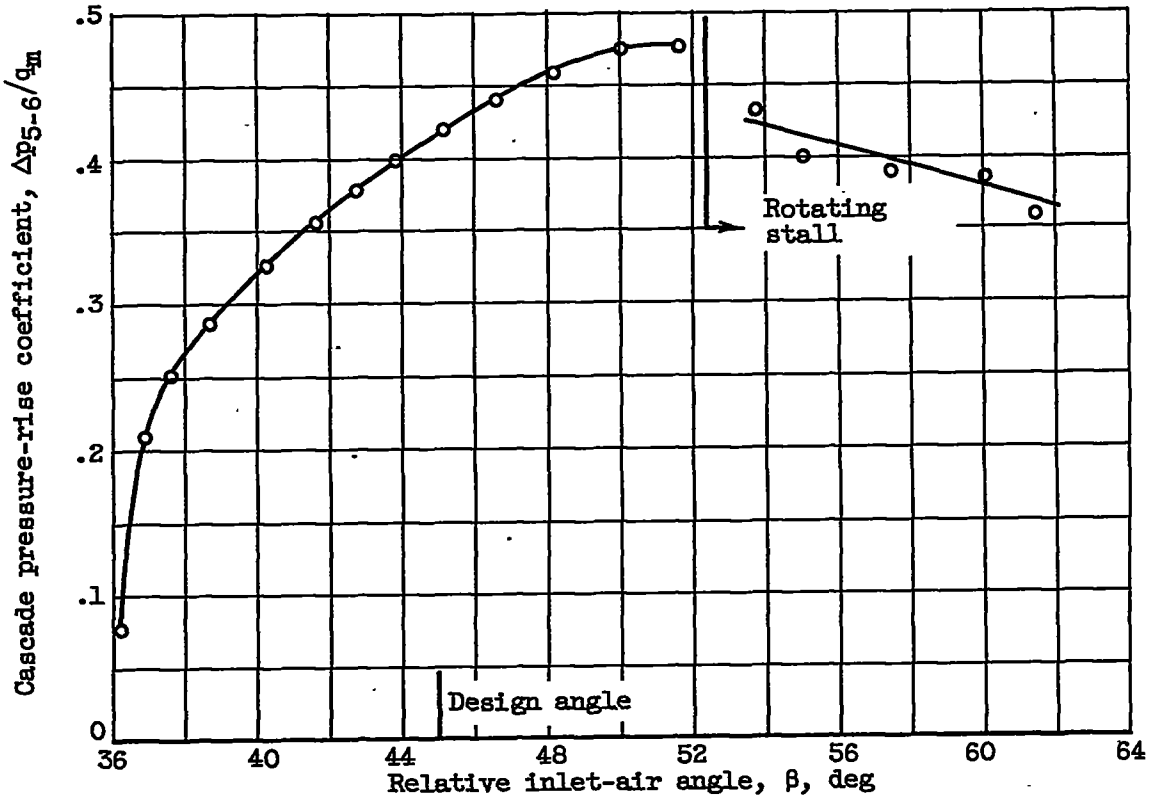

(i) Configuration 9. Guide-vane turning angle, none; no stators; corrected rotor speed, 8000 rpm.

Figure 6. - Concluded. Rotor pressure-rise characteristic as function of relative inlet-air angle at mean radius ratio of 0.95.

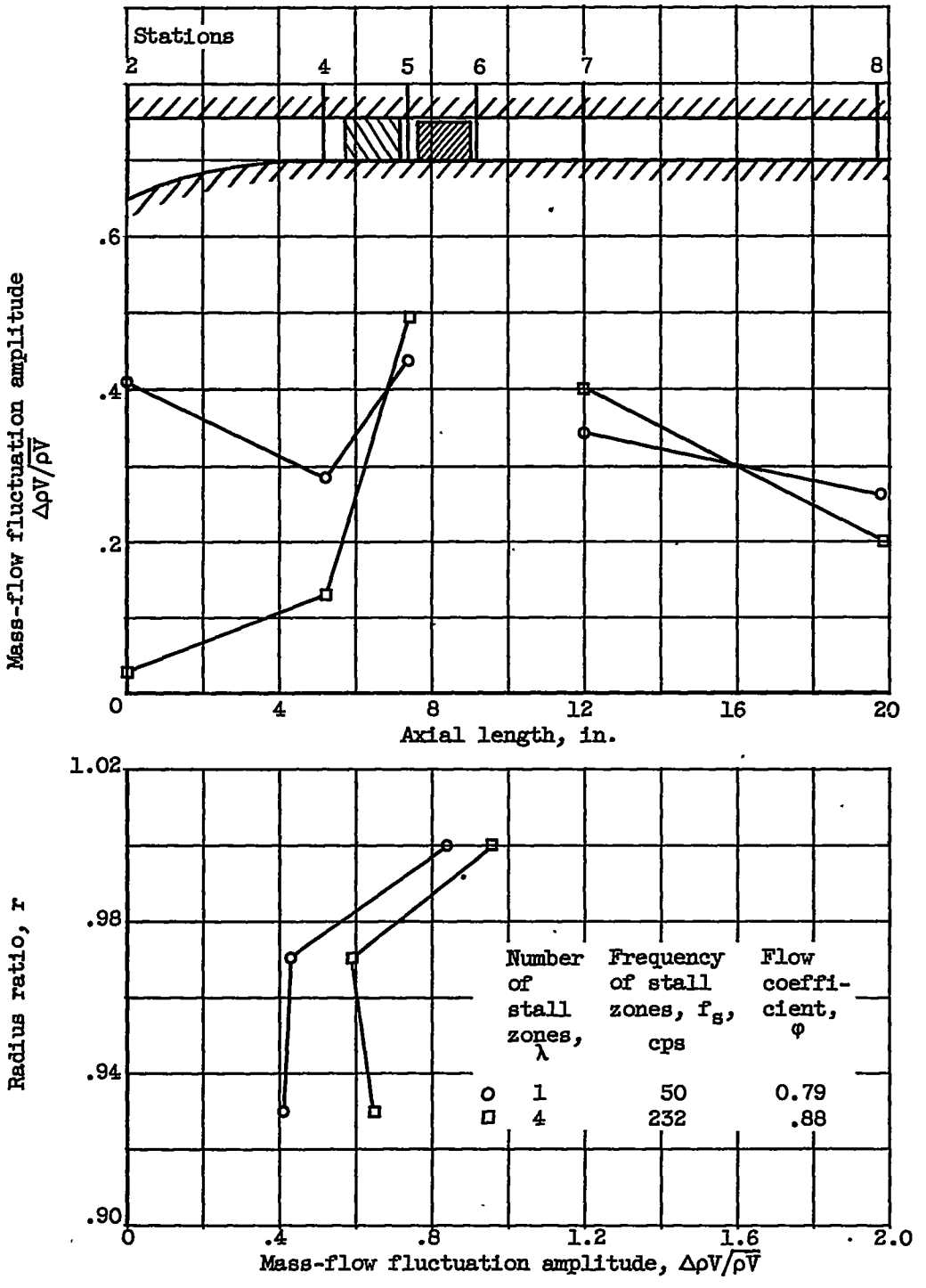

(a) Configuration 1. Guide-vane turning angle, -22.5°; no stators; corrected rotor speed, 8000 rpm; radial survey at station 5; axial survey along stage axis.

Figure 7. - Flow fluctuation amplitudes.

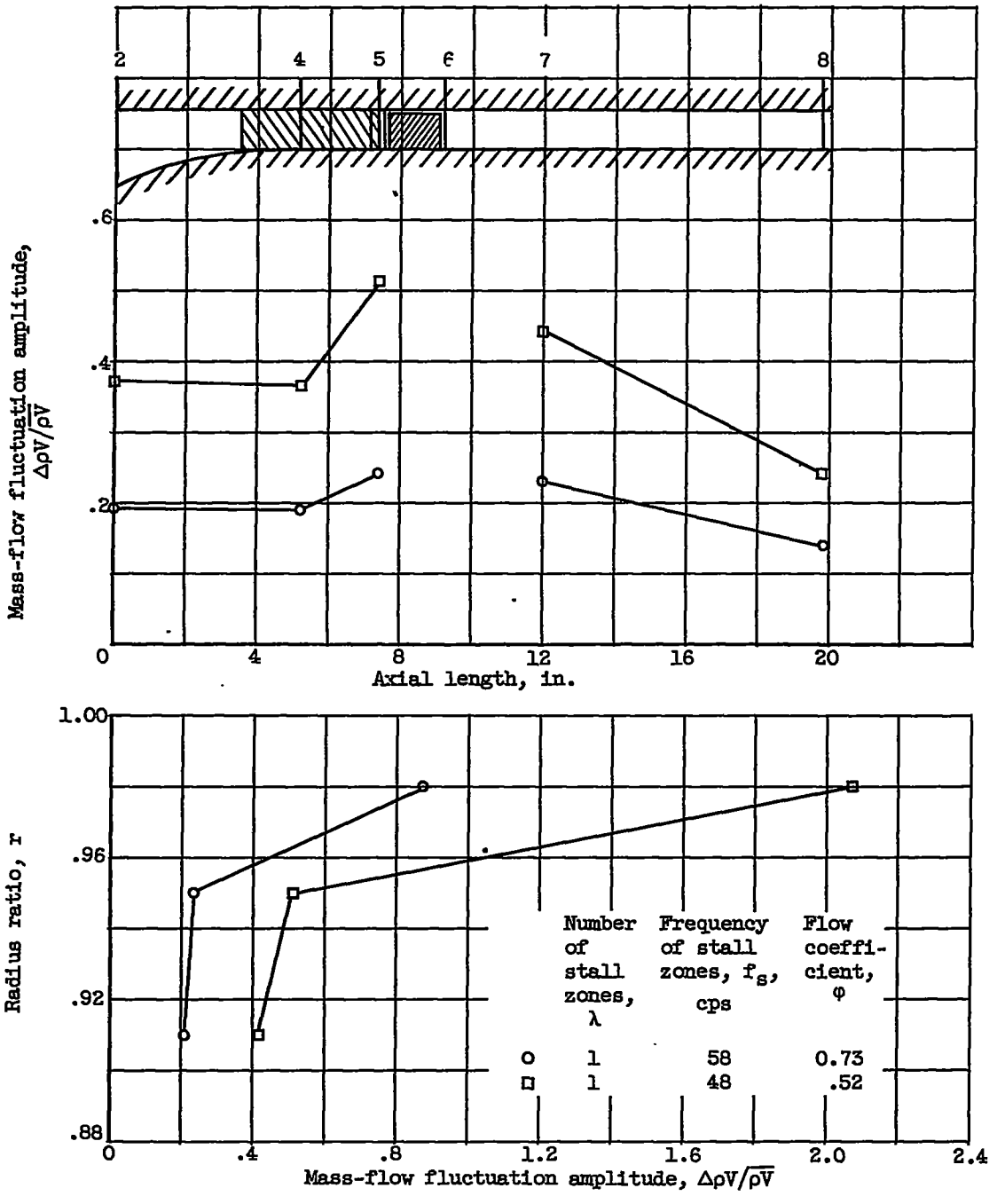

(b) Configuration 2. Guide-vane turning angle, 0°; no stators; corrected rotor speed, 8000 rpm; radial survey at station 5; axial survey along stage axis.

Figure 7. - Continued. Flow fluctuation amplitudes.

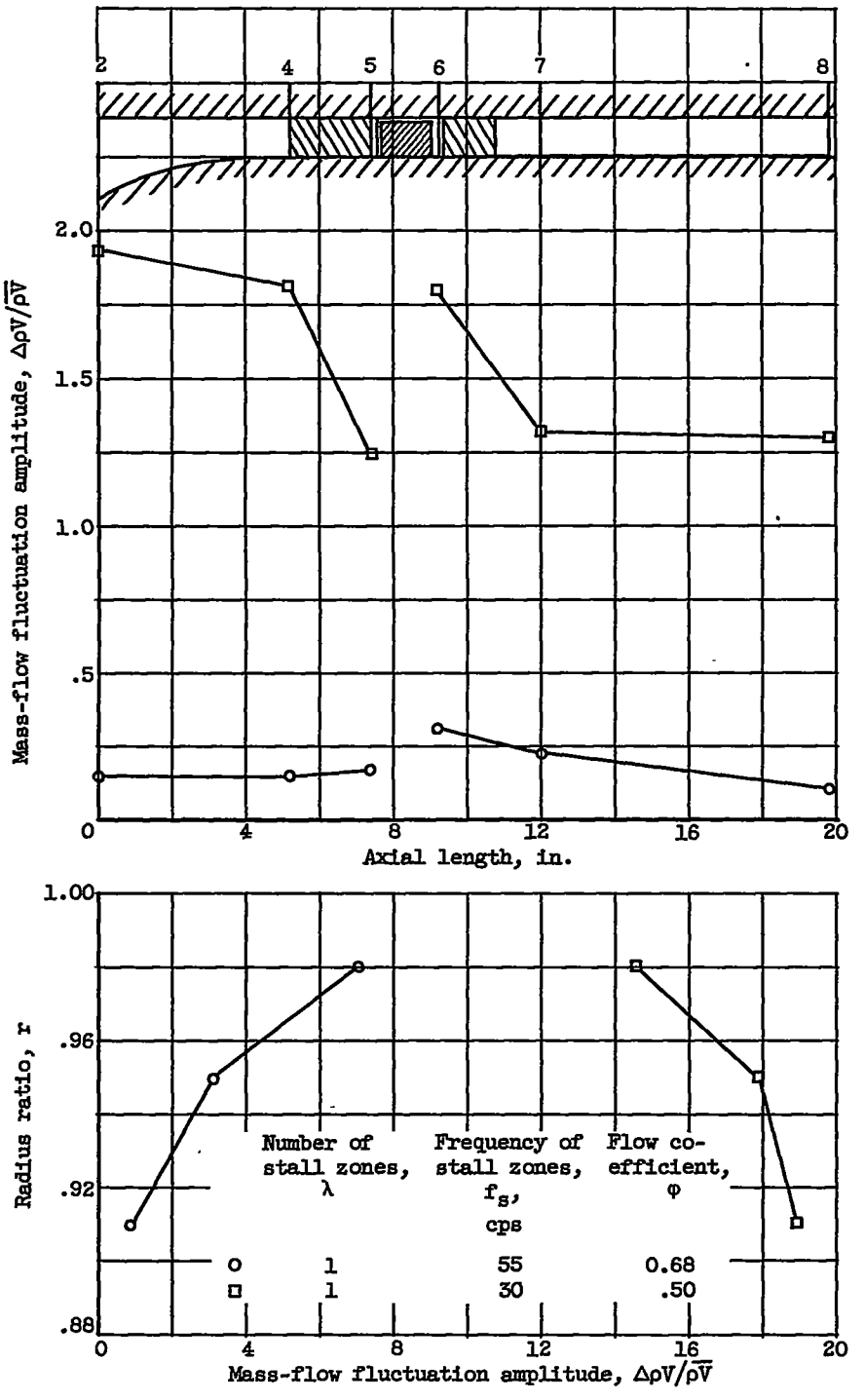

(c) Configuration 3. Guide-vane turning angle, 0°; stators; corrected rotor speed, 8000 rpm; radial survey at station 6; axial survey along stage axis.

Figure 7. - Continued. Flow fluctuation amplitudes.

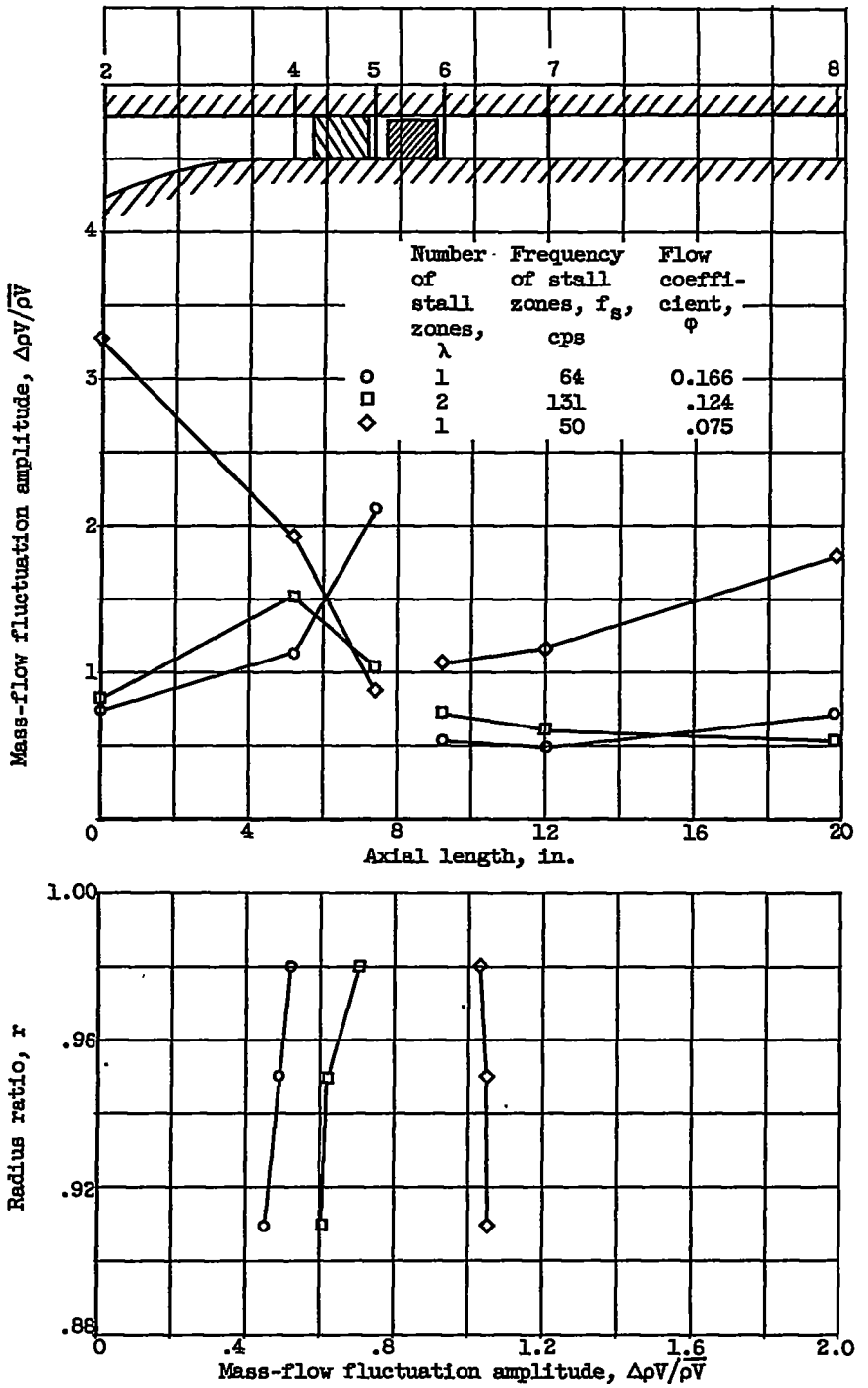

(d) Configuration 4. Guide-vane turning angle, 22.5°; no stators; corrected rotor speed, 10,000 rpm; radial survey at station 6; axial survey along stage axis.

Figure 7. - Continued. Flow fluctuation amplitudes.

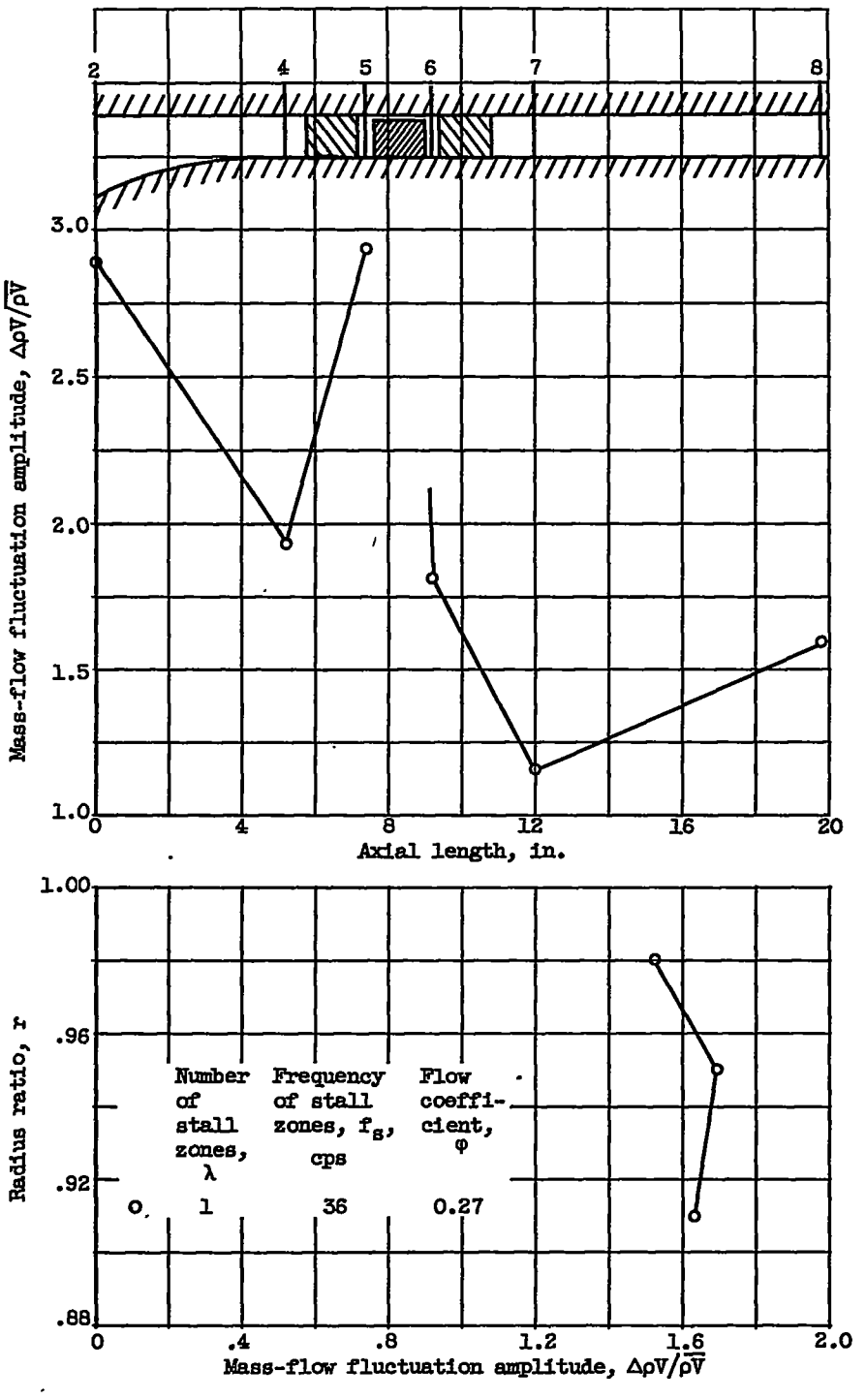

(e) Configuration 5. Guide-vane turning angle, 22.5°; stators; corrected rotor speed, 10,000 rpm; radial survey at station 6; axial survey along stage axis.

Figure 7. - Continued. Flow fluctuation amplitudes.

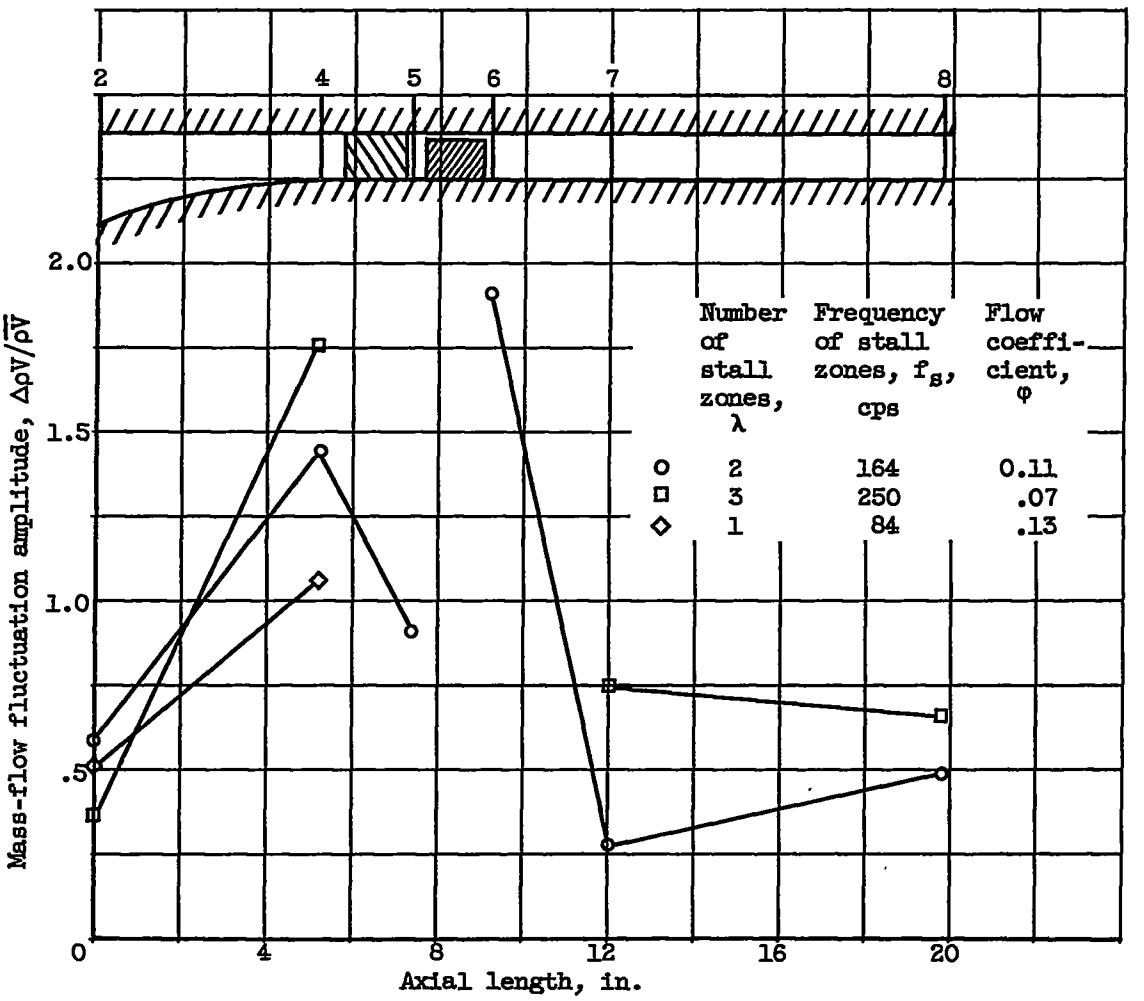

(f) Configuration 7. Guide-vane turning angle, 40°; no stators; corrected rotor speed, 12,000 rpm; radial survey, no data obtained.

Figure 7. - Continued. Flow fluctuation amplitudes.

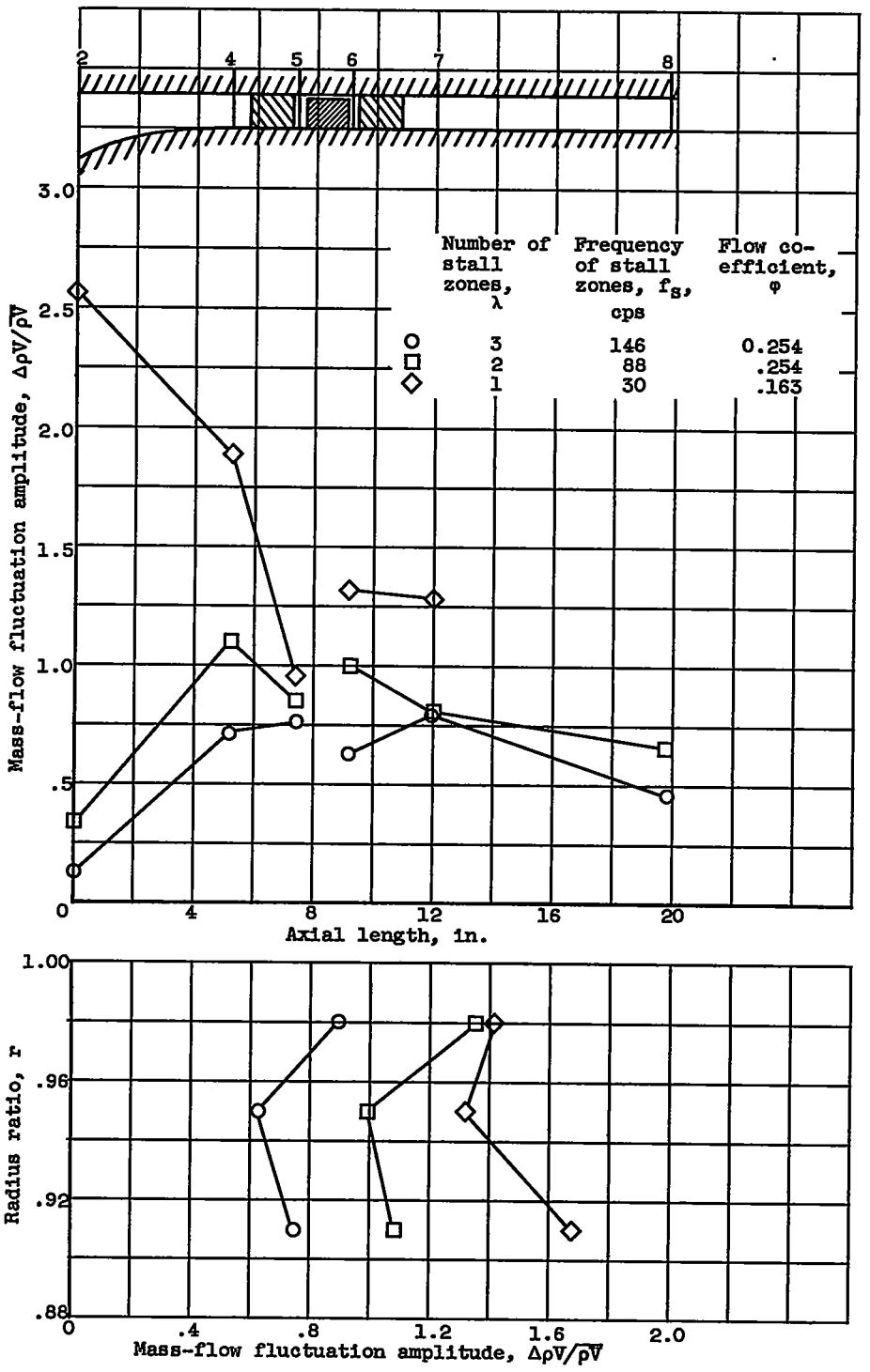

(g) Configuration 8. Guide-vane turning angle, 40°; stators; corrected rotor speed, 8000 rpm; radial survey at station 6; axial survey along stage axis.

Figure 7. - Continued. Flow fluctuation amplitudes.

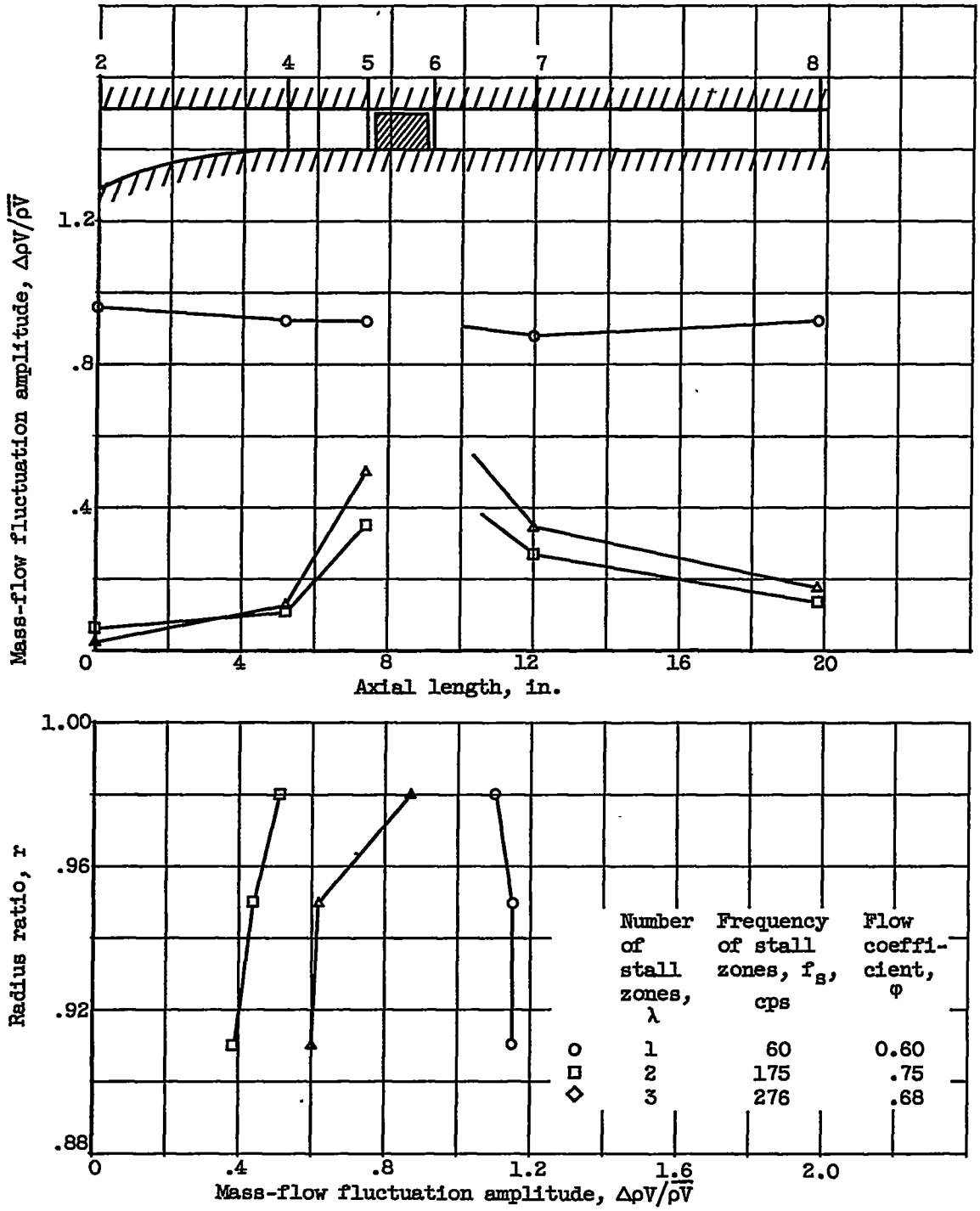

(h) Configuration 9. Rotor alone; radial survey at station 5; axial survey along stage axis.

Figure 7. - Concluded. Flow fluctuation amplitudes.

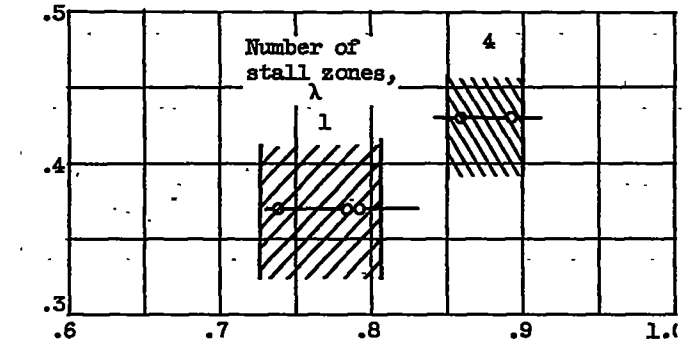

(a) Configuration 1.

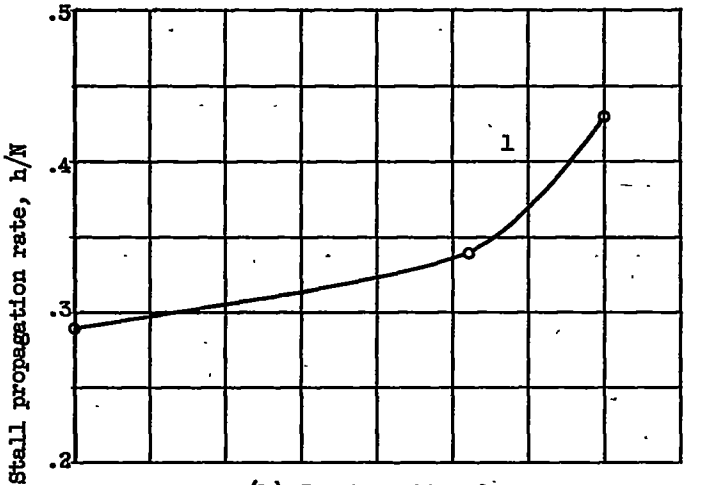

(b) Configuration 2.

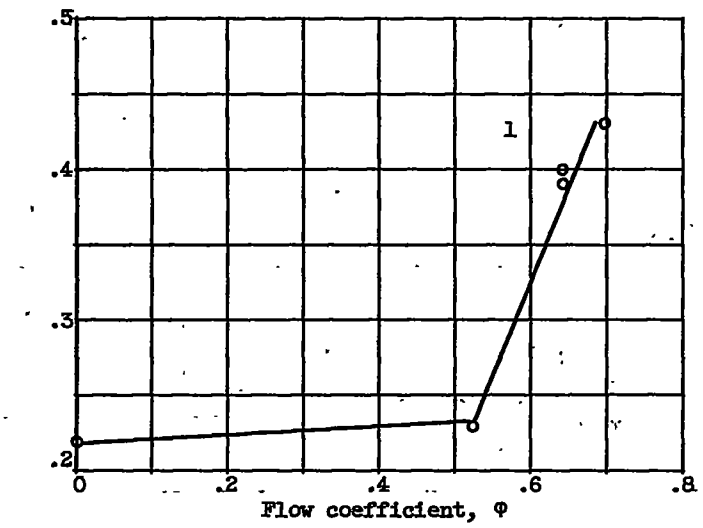

(c) Configuration 3.

Figure 8. - Stall propagation rate as a function of flow coefficient.

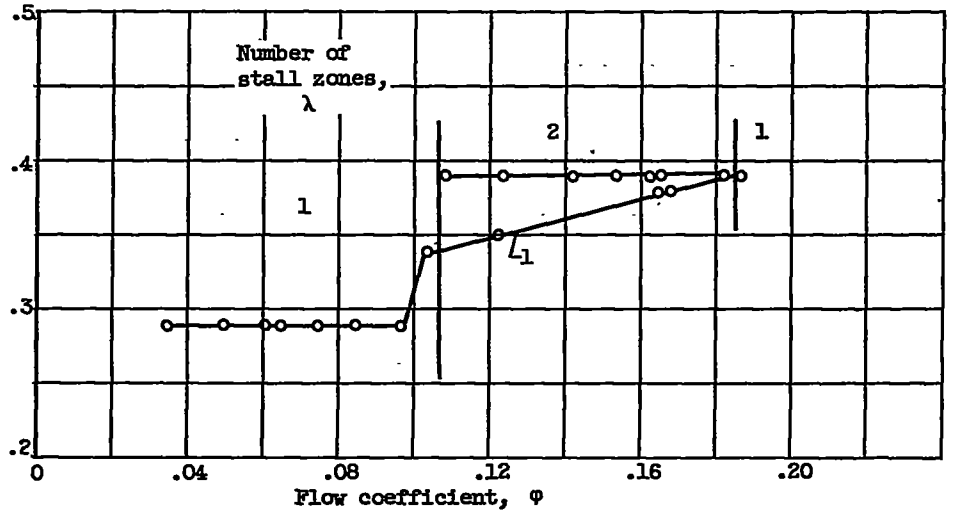

(d) Configuration 4.

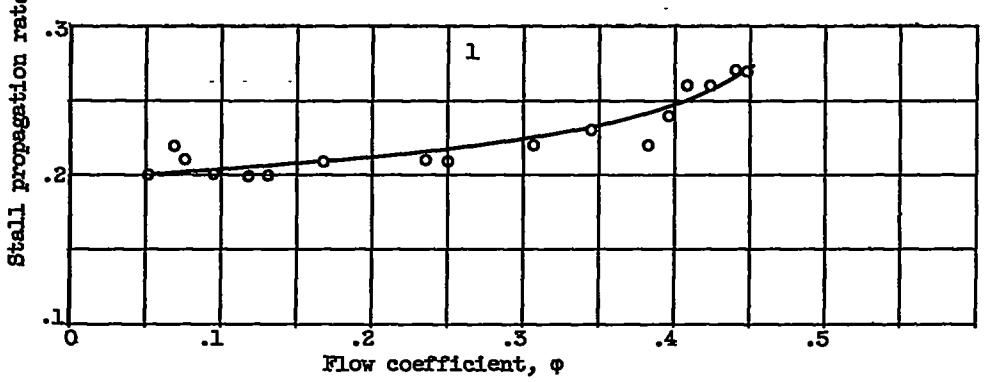

(e) Configuration 5.

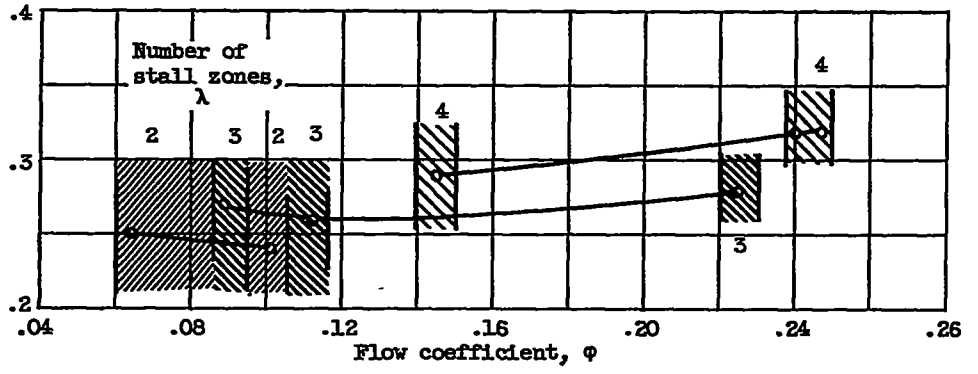

(f) Configuration 6.

Figure 8. - Continued. Stall propagation rate as a function of flow coefficient.

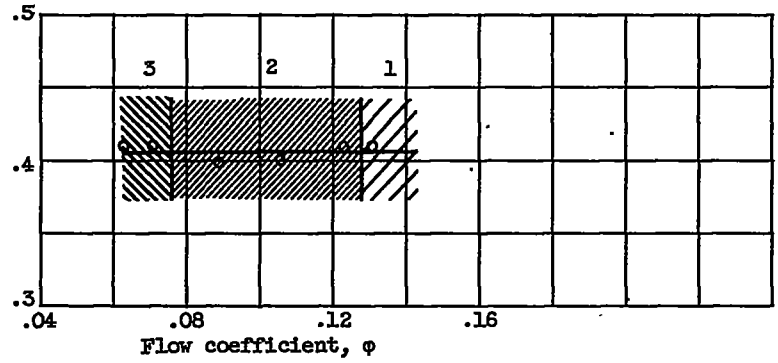

(g) Configuration 7.

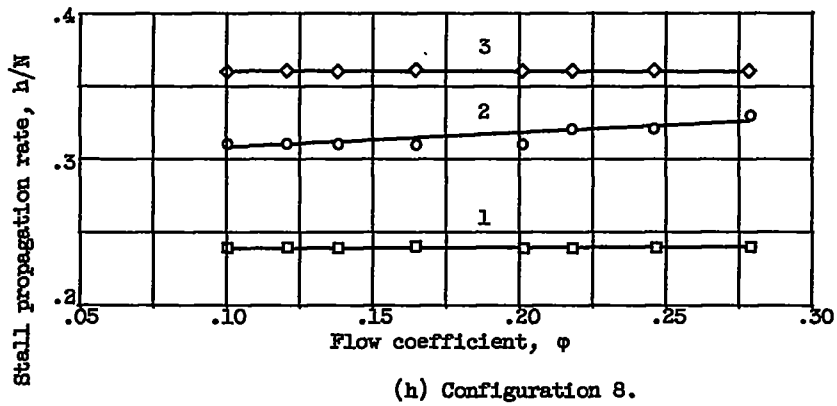

(h) Configuration 8.

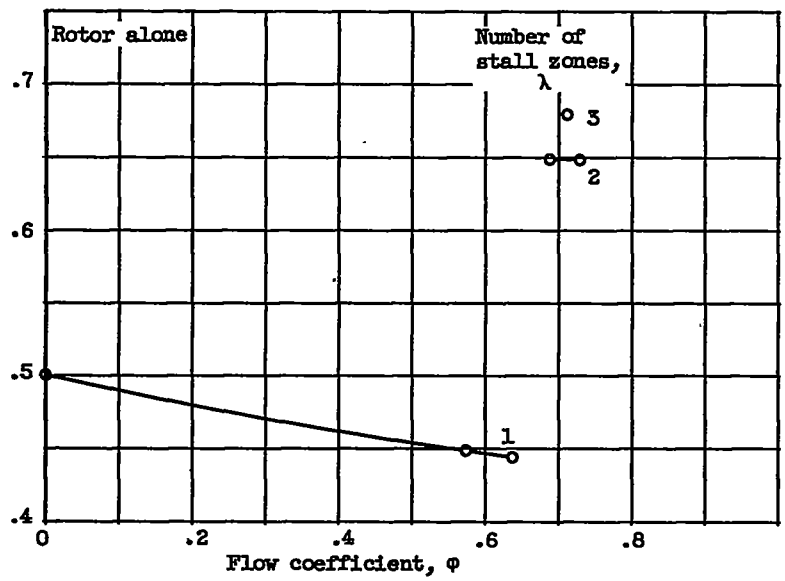

(i) Configuration 9.

Figure 8. - Concluded. Stall propagation rate as a function of flow coefficient.

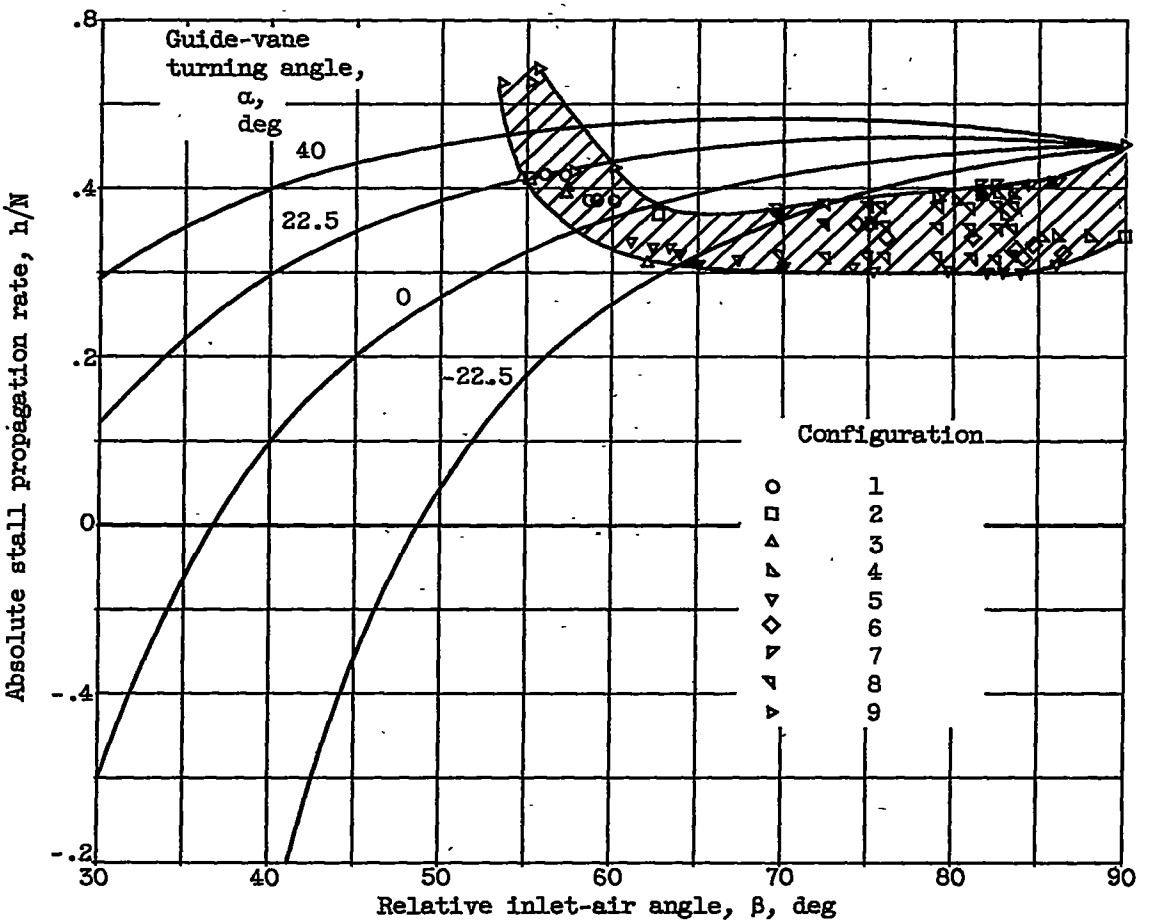

Figure 9. - Stall propagation rates for all configurations compared with those for simple cascade equation (ref. 10).